Carbon Nanostructures

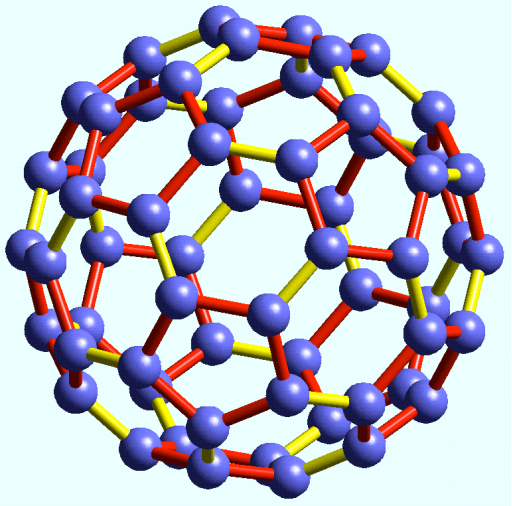

- C_{60}, buckminsterfullerene, buckyball
  - (1985) Kroto, Heath, O'Brien, Curl, Smalley, *Nature* **318**, 162-163.
- Carbon nanotubes
  - (1991) Sumio Iijima, *Nature* **354**, 56-58.

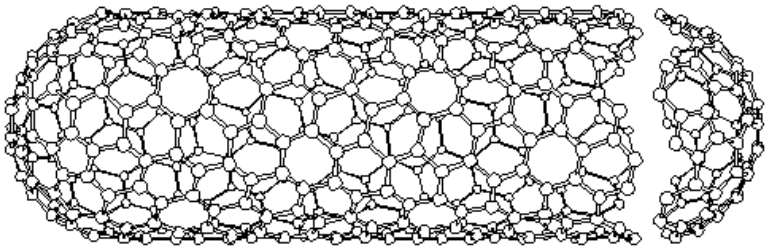

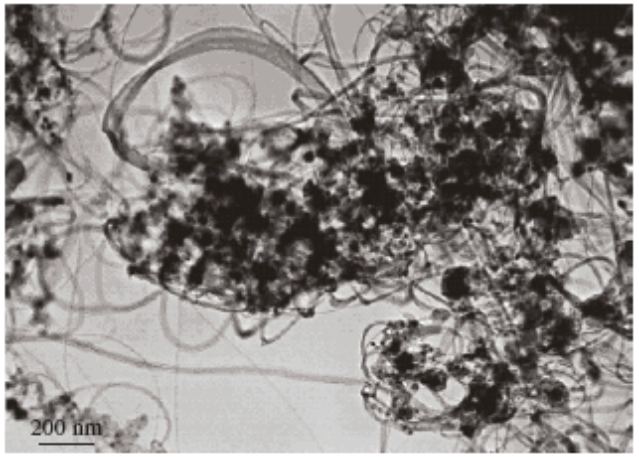

Fig. 3.11 Low magnification TEM images of a typical raw SWNT material obtained from the laser vaporization technique. Fibrous morphologies are SWNT bundles, and dark particles are catalyst remnants. Raw SWNT materials from electric arc exhibit a similar aspect (from [3.14])

C_{60}

(1985) Kroto, Heath, O'Brien, Curl, Smalley, *Nature* **318**, 162-163.

C_{60}: Buckminsterfullerene

H. W. Kroto*, J. R. Heath, S. C. O'Brien, R. F. Curl & R. E. Smalley

Rice Quantum Institute and Departments of Chemistry and Electrical Engineering, Rice University, Houston, Texas 77251, USA

During experiments aimed at understanding the mechanisms by which long-chain carbon molecules are formed in interstellar space and circumstellar shells[1], graphite has been vaporized by laser irradiation, producing a remarkably stable cluster consisting of 60 carbon atoms. Concerning the question of what kind of 60-carbon atom structure might give rise to a superstable species, we suggest a truncated icosahedron, a polygon with 60 vertices and 32 faces, 12 of which are pentagonal and 20 hexagonal. This object is commonly encountered as the football shown in Fig. 1. The C_{60} molecule which results when a carbon atom is placed at each vertex of this structure has all valences satisfied by two single bonds and one double bond, has many resonance structures, and appears to be aromatic.

Fig. 1 A football (in the United States, a soccerball) on Texas grass. The C_{60} molecule featured in this letter is suggested to have the truncated icosahedral structure formed by replacing each vertex on the seams of such a ball by a carbon atom.

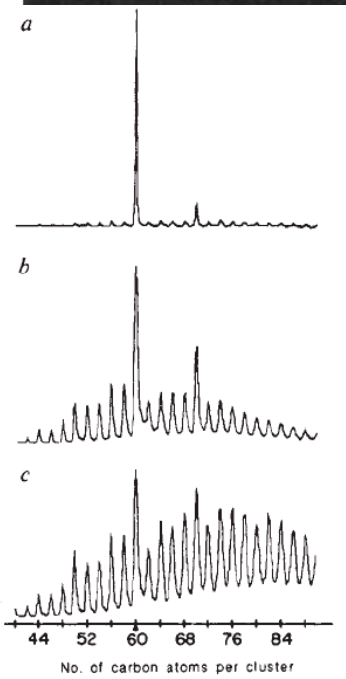

760 torr He

10 torr He

Fig. 3 Time-of-flight mass spectra of carbon clusters prepared by laser vaporization of graphite and cooled in a supersonic beam.

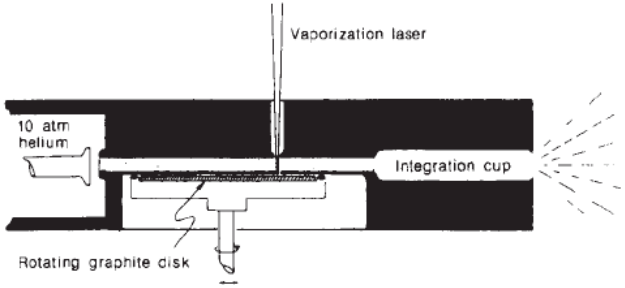

Helical microtubules of graphitic carbon

(1991) Sumio Iijima, *Nature* **354**, 56-58.

CNT, Iijima, 1991

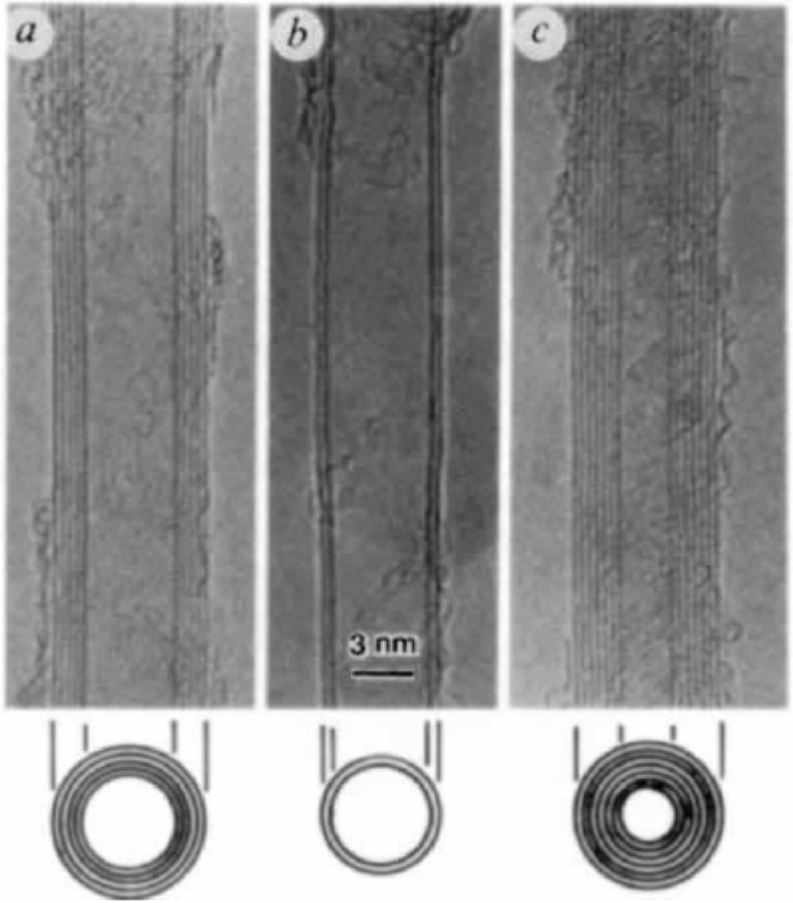

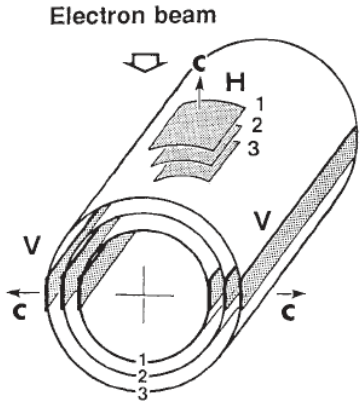

FIG. 2 Clinographic view of a possible structural model for a graphitic tubule. Each cylinder represents a coaxial closed layer of carbon hexagons. The meaning of the labels V and H is explained in the text.

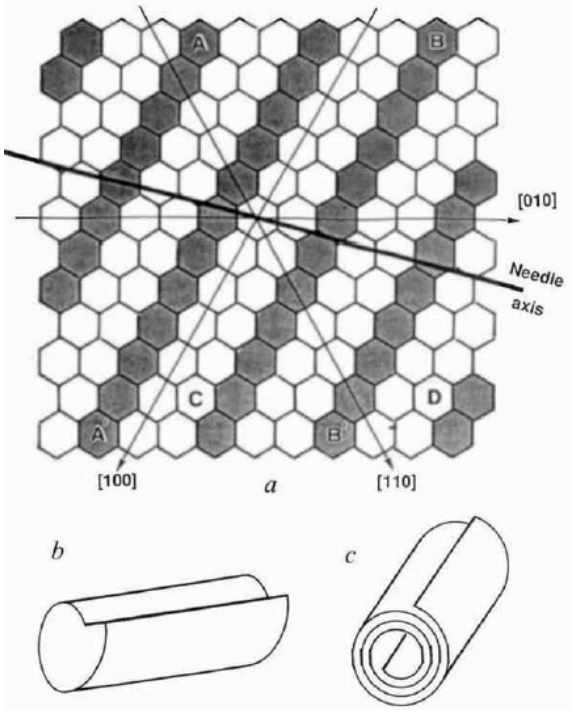

NATURE | VOL 408 | 2 NOVEMBER 2000 |

CNT smallest tubes

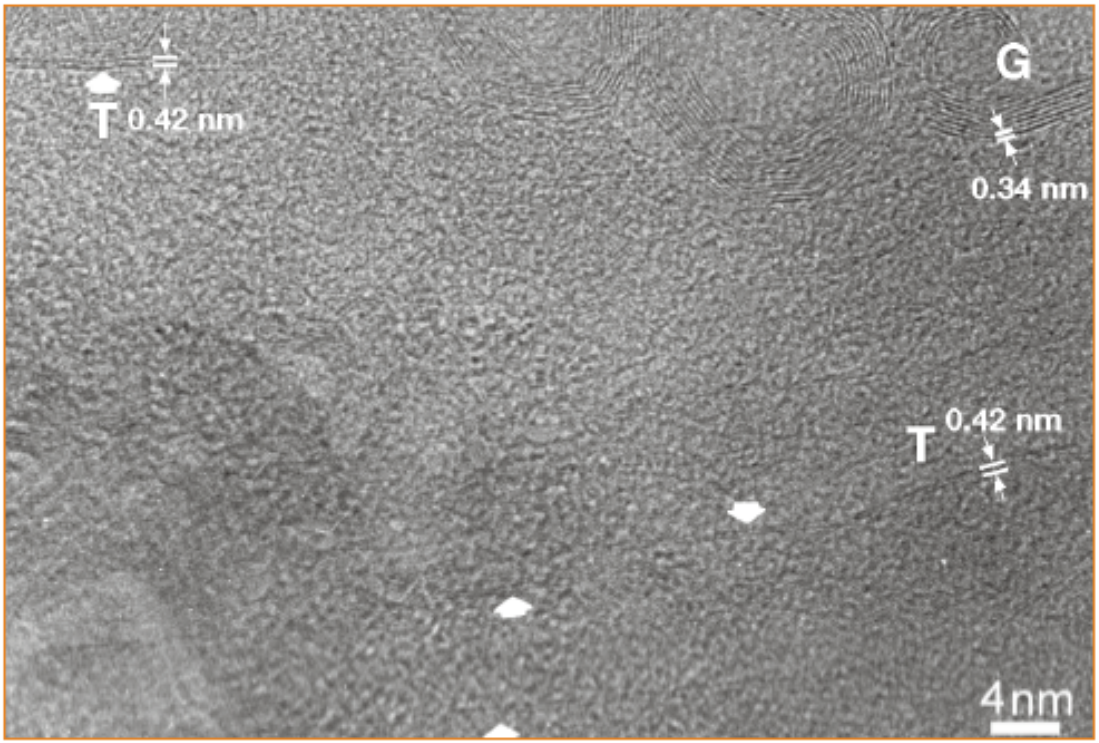

Figure 2 High-resolution transmission electron microscope image showing single-walled carbon nanotubes (indicated by T and large arrowheads) coexisting with graphite in raft-like stripes (G). More than ten single-walled carbon nanotubes are visible.

Figure 1 High-resolution electron microscope image of a 4 Å tubule (side walls are marked by lines) confined inside an 18-shell carbon nanotube. Dark lines correspond to the side

C_{20} tubes, 4Å wide, always armchair, always metallic

CNT Synthesis

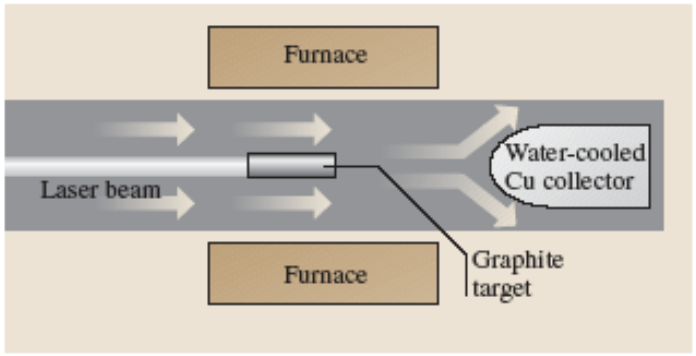

Fig. 3.9 Sketch of an early laser vaporization apparatus

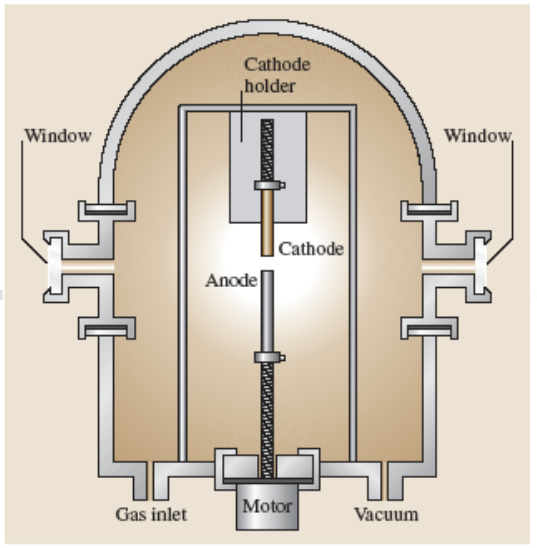

Fig. 3.12 Sketch of an electric arc reactor

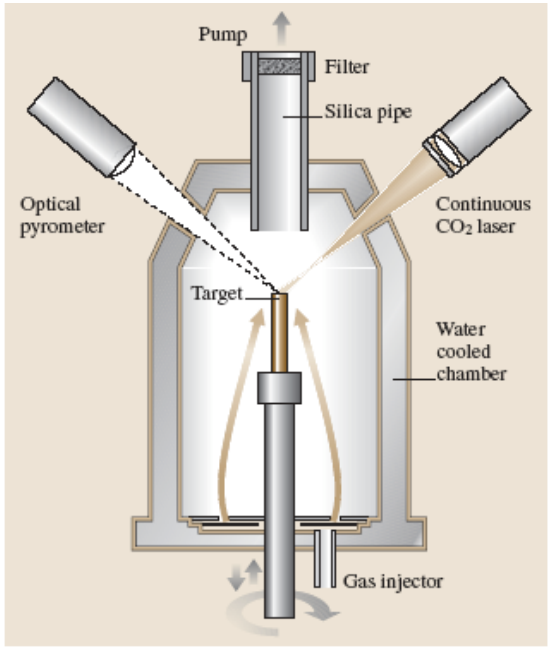

Fig. 3.10 Sketch of a synthesis reactor with a continuous CO_2 laser device (adapted from [3.26])

- Laser
- Electric arc
- Solar
- CVD

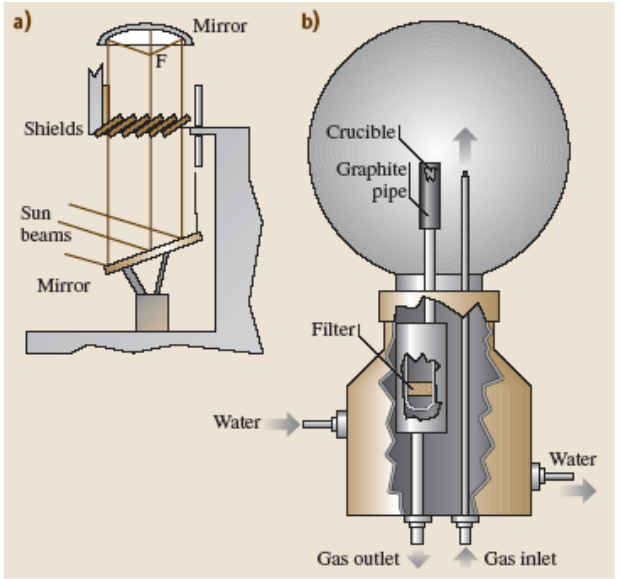

Fig. 3.14a,b Sketch of a solar energy reactor in use in Odeilho (France). **(a)** Gathering of sun rays, focused in F; **(b)** Example of Pyrex® chamber placed in **(a)** so that the graphite crucible is at the point F (adapted from [3.56])

CNT synthesis mechanism

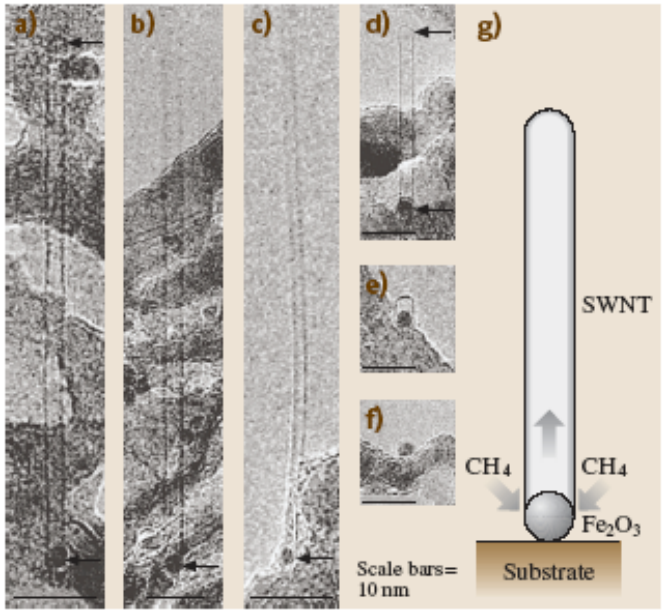

Fig. 3.20 High resolution transmission electron microscopy images of several SWNTs grown from iron-based nanoparticles by CCVD method, showing that particle sizes determine SWNT diameters in that case (adapted from [3.116])

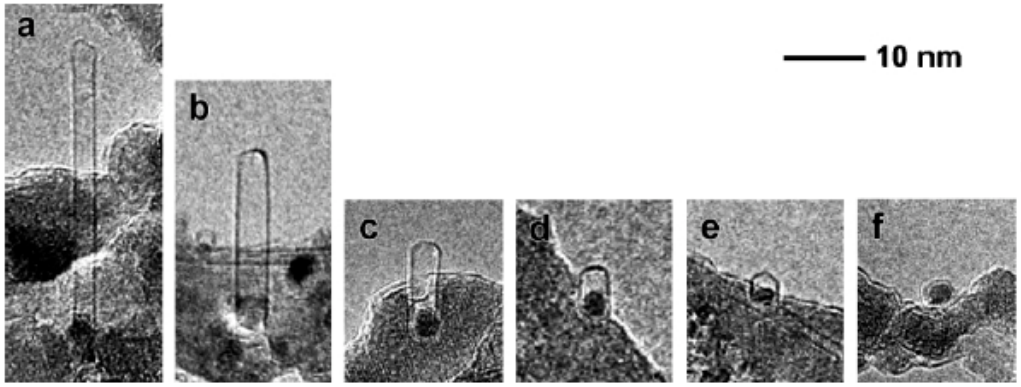

- Large catalyst particles
- Surface bound NP catalyst
  - (from ferritin)
- "Kiting" NP catalyst

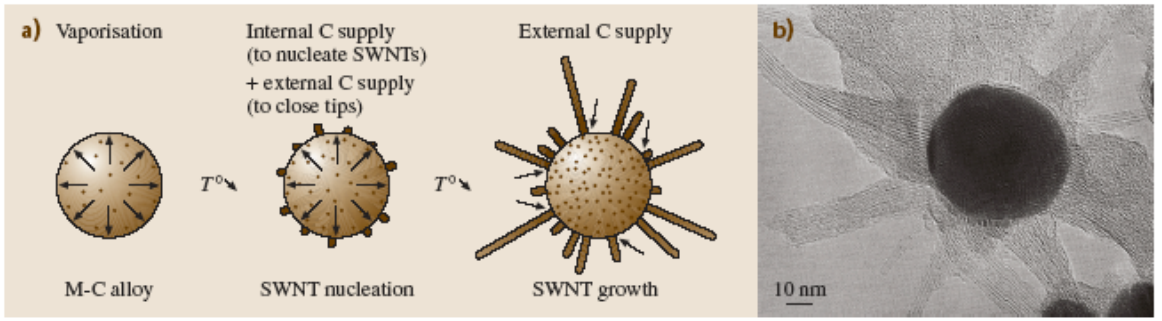

Fig. 3.21 (a) Mechanism proposed for SWNT growth (see text). (b) Transmission electron microscopy image of SWNT growing radial to a large Ni catalyst particle surface in the electric arc experiment. (modified from [3.17])

Protein based catalyst - Ferritin

Growth of Single-Walled Carbon Nanotubes from Discrete Catalytic Nanoparticles of Various Sizes

Yiming Li, Woong Kim, Yuegang Zhang, Marco Rolandi, Dunwei Wang, and Hongjie Dai*

Department of Chemistry, Stanford University, Stanford, California 94305

J. Phys. Chem. B, Vol. 105, No. 46, 2001 **11425**

Appl. Phys. A 74, 325–328 (2002)

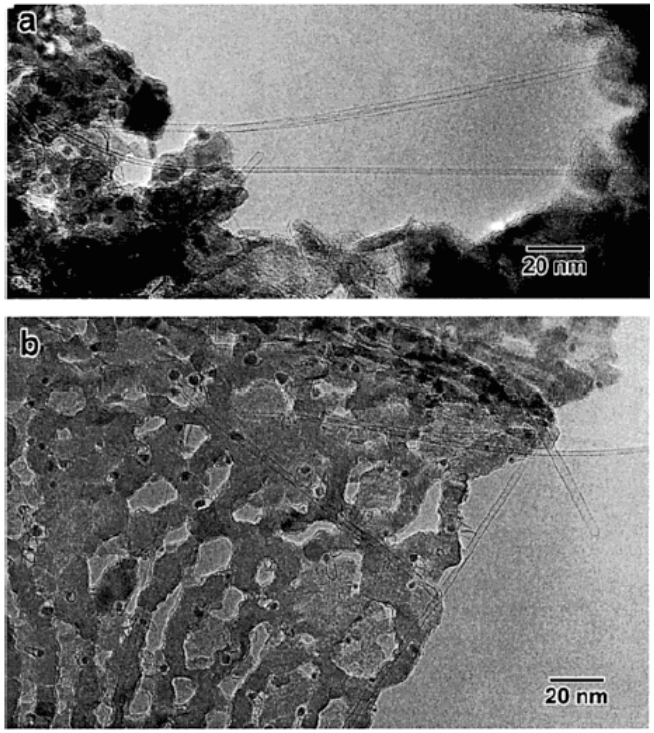

Figure 6. TEM images of SWNTs as grown on ultrathin alumina membranes formed directly on TEM micro-grids. (a) A TEM image showing the synthesized SWNTs. (b) A TEM image showing SWNTs and discrete nanoparticles (black dots) on the porous alumina membrane.

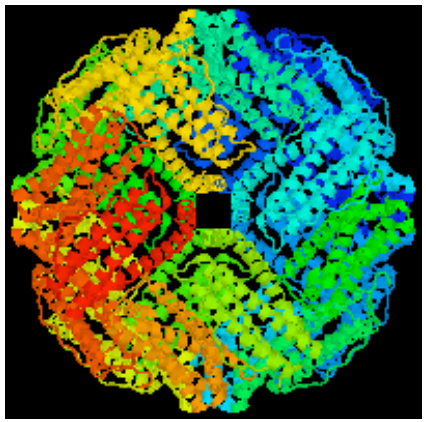

SCHEME 1. Process Flow for SWNT Synthesis from Discrete Nanoparticles by CVD

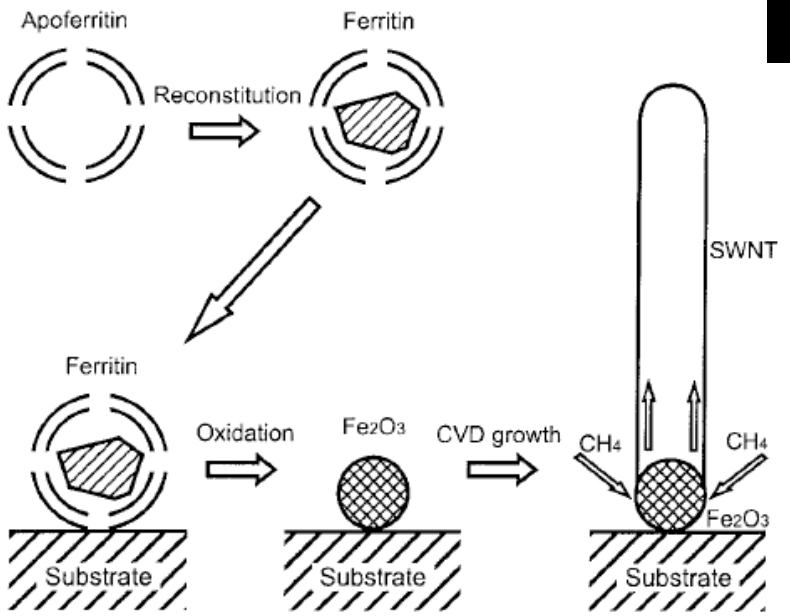

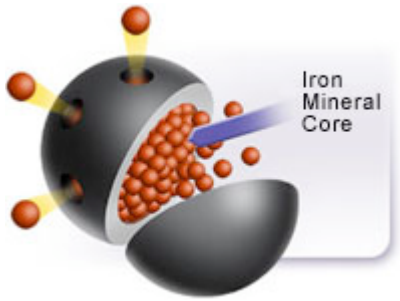

CNT, etc.

- Filling
- Organization

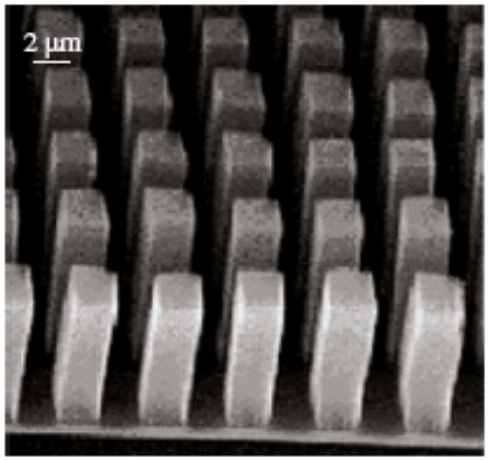

Fig. 3.17 Example of a free-standing MWNT array obtained from the pyrolysis of a gaseous carbon source over catalyst nanoparticles previously deposited onto a patterned substrate. Each square-base rod is a bunch of MWNTs aligned perpendicular to the surface (from [3.97])

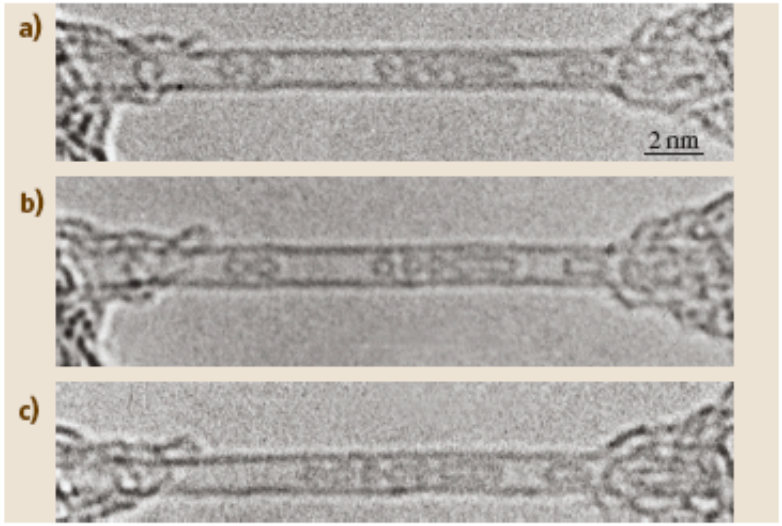

Fig. 3.26a–c HRTEM images of (a) example of five regular C_{60} molecules encapsulated together with two higher fullerenes (C_{120} and C_{180}) as distorted capsules (*on the right*) within a regular 1.4 nm diameter SWNT. (a)–(c) Example of the diffusion of the C_{60}-

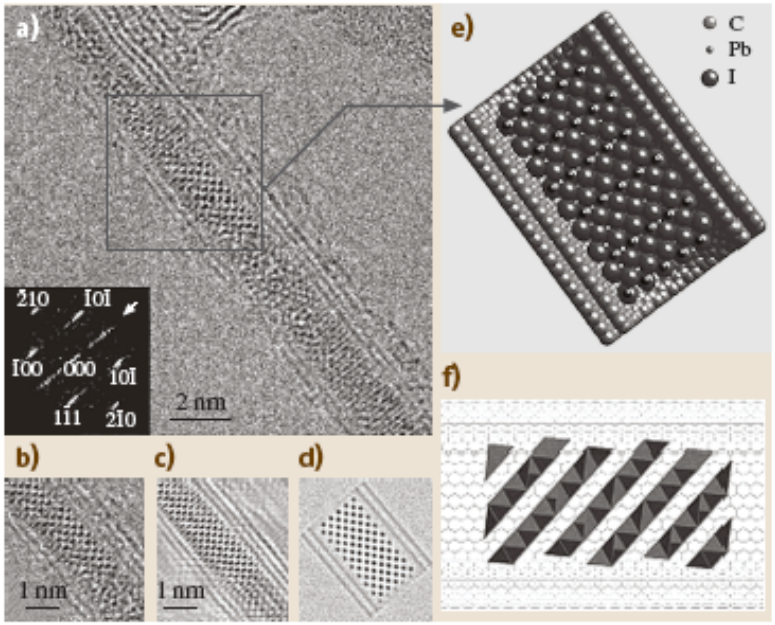

Fig. 3.25 HRTEM images (experimental and simulations), and corresponding structural model for a PbI_2 filled double-wall carbon nanotube (from [3.186])

Doped CNT

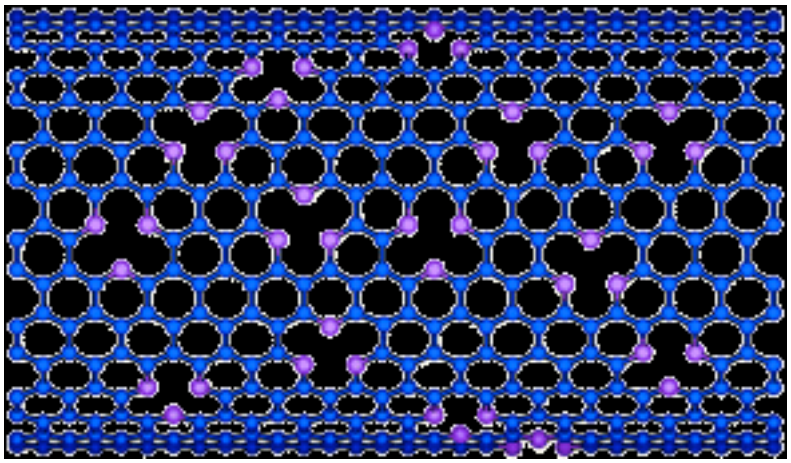

- N doped
- B doped

Single-Wall Carbon Nanotubes for Nanoelectronics & Biosensors

- SWNT devices
- SWNT circuits
- Interactions with proteins and DNA
- Self-assembly using DNA
- Biosensors from protein/CNT

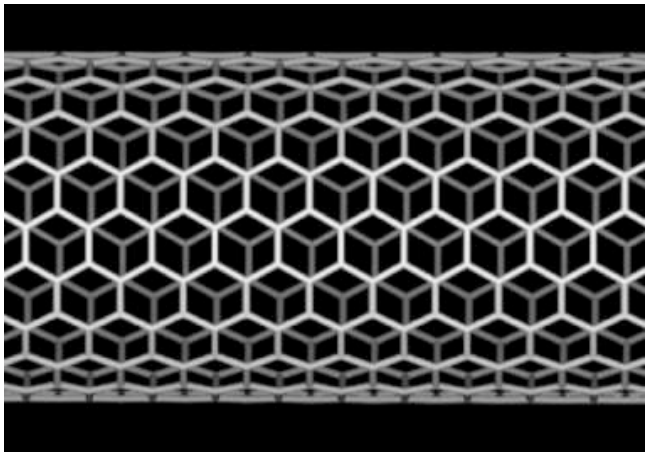

(10,10) SWNT

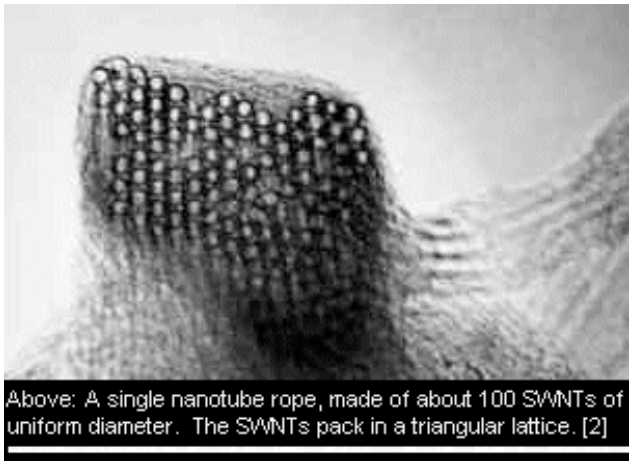

Above: A single nanotube rope, made of about 100 SWNTs of uniform diameter. The SWNTs pack in a triangular lattice. [2]

SWNT, some properties

- n,m vector
- n,0 zigzag
- n,n armchair
- Other = chiral
- n-m is divisible by 3
  tube is metallic

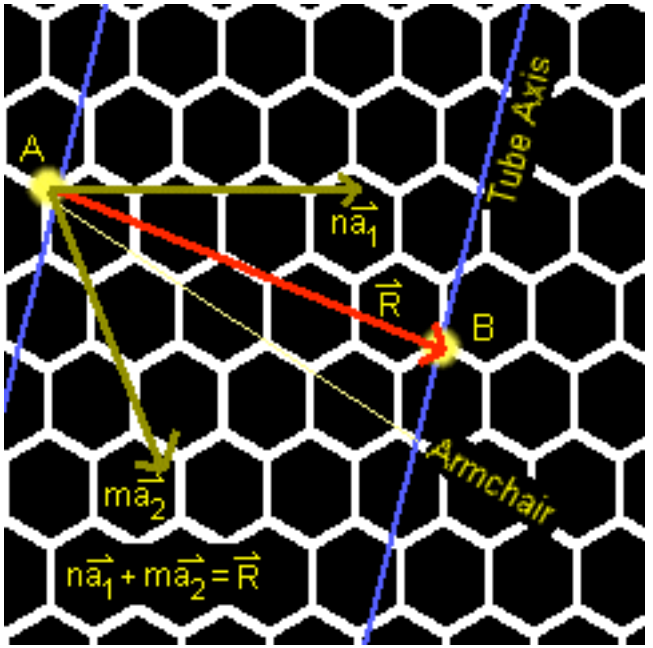

http://www.pa.msu.edu/cmp/csc/nanotube.html

Carbon nanotubes: nanomechanics, manipulation, and electronic devices

Ph. Avouris *, T. Hertel, R. Martel, T. Schmidt, H.R. Shea, R.E. Walkup

IBM Research Division, T.J. Watson Research Center, Yorktown Heights, NY 10598, USA

Applied Surface Science 141 (1999) 201–209

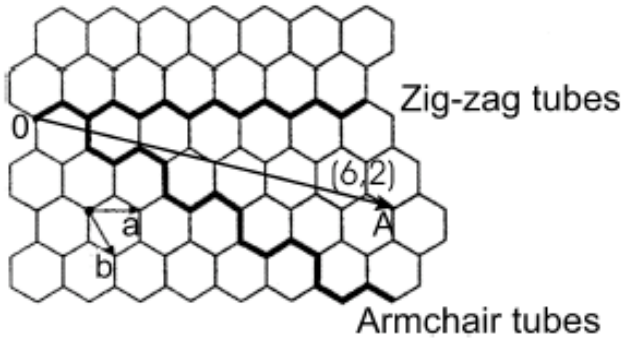

Fig. 1. A graphene sheet with unit vectors a and b. A nanotube can be formed by folding the sheet so that the end points O and A of the vector $C = na + mb = (n,m)$ coincide. When $n = m$, the ends of the tube have a meander-like structure and the tube is called an armchair tube. When $n = 0$, the ends of the nanotube have a zig-zag structure. Nanotubes with arbitrary values of n and m have a chiral structure.

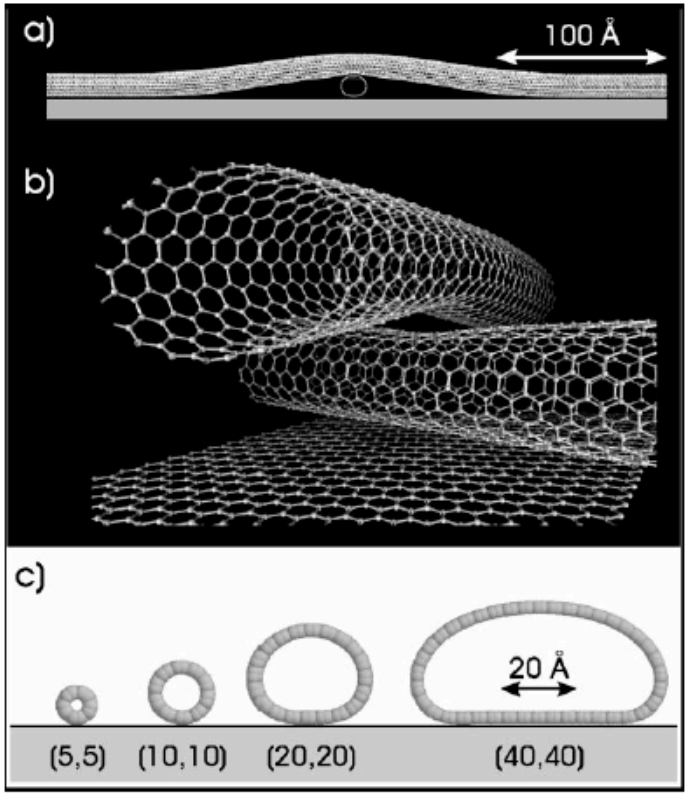

Fig. 3. Molecular mechanics calculations on the axial and radial deformations of single-wall carbon nanotubes. (a) Axial deformation resulting from the crossing of two (10,10) nanotubes. (b) Perspective close up of the same crossing showing that both tubes are deformed near the contact region. The force acting on the lower tube is about 5 nN. (c) Computed radial deformations of single-wall nanotubes on graphite.

AFM manipulation of CNT

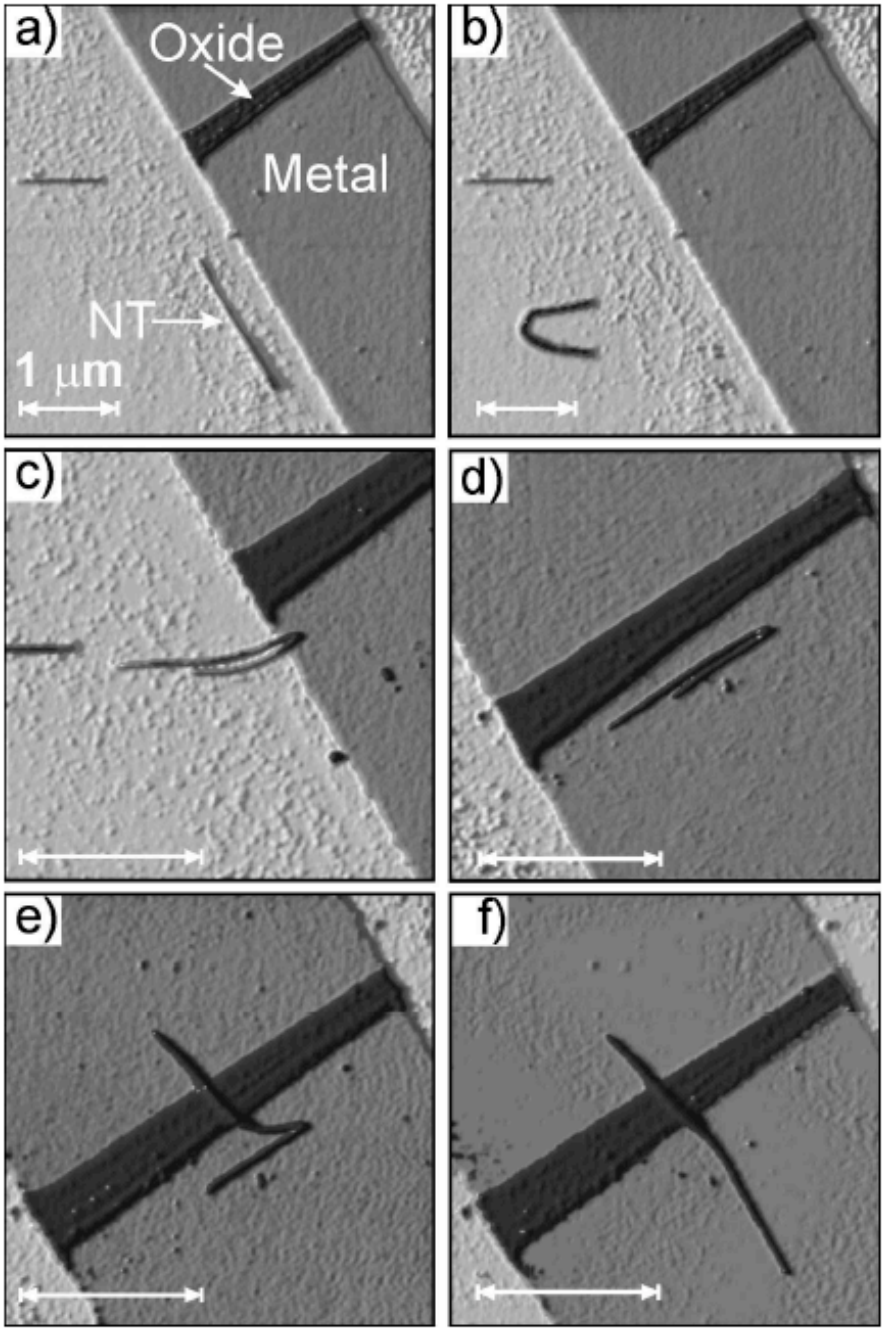

Carbon nanotubes: nanomechanics, manipulation, and electronic devices

Ph. Avouris *, T. Hertel, R. Martel, T. Schmidt, H.R. Shea, R.E. Walkup

IBM Research Division, T.J. Watson Research Center, Yorktown Heights, NY 10598, USA

Applied Surface Science 141 (1999) 201–209

Targeted deposition of CNT

Controlled deposition of individual single-walled carbon nanotubes on chemically functionalized templates

Jie Liu, Michael J. Casavant, Michael Cox, D.A. Walters, P. Boul, Wei Lu, A.J. Rimberg, K.A. Smith, Daniel T. Colbert *, Richard E. Smalley

Center for Nanoscale Science and Technology, Rice Quantum Institute, and Department of Chemistry and Physics, Rice University, 6100 S. main Street, Houston, TX 77005, USA

Chemical Physics Letters 303 (1999) 125–129

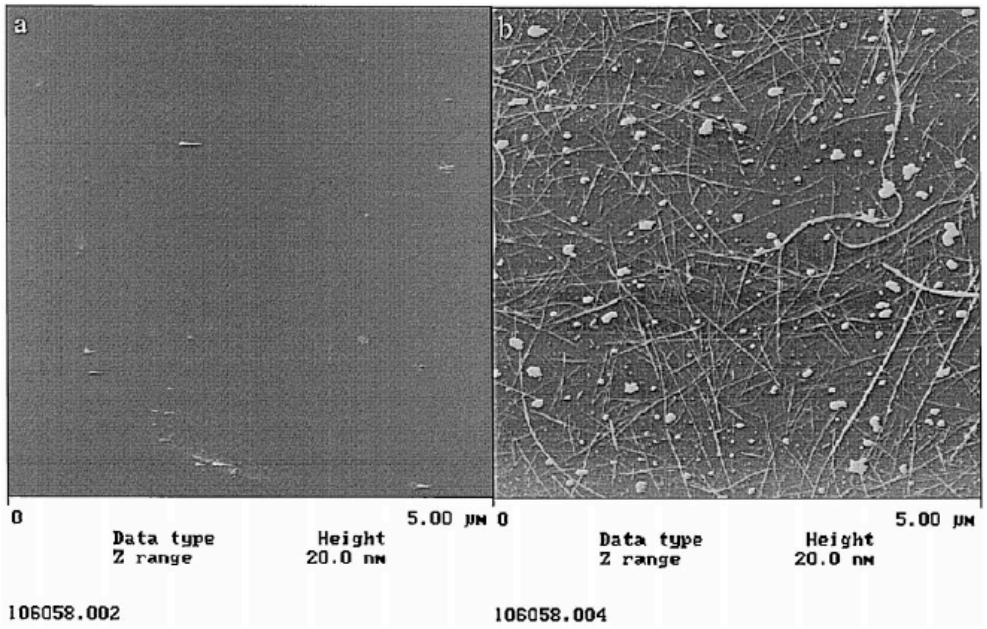

Fig. 2. Tapping mode AFM images of: (a) $-CH_3$ functionalized SiO_2 surface and (b) $-NH_2$ functionalized surfaces after soaking in SWNT/DMF suspension for 10 min and rinsing with methanol.

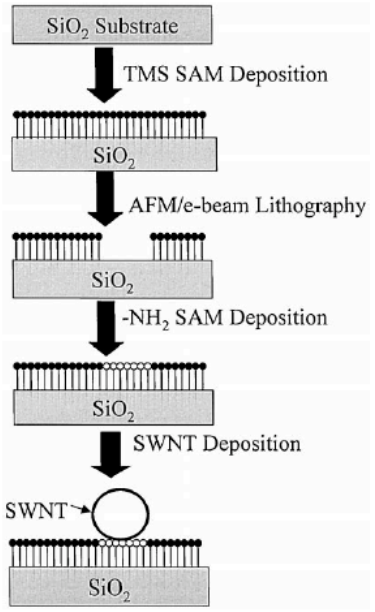

Fig. 3. Schematic diagram of controlled deposition of SWNT on chemically functionalized lithographic patterns.

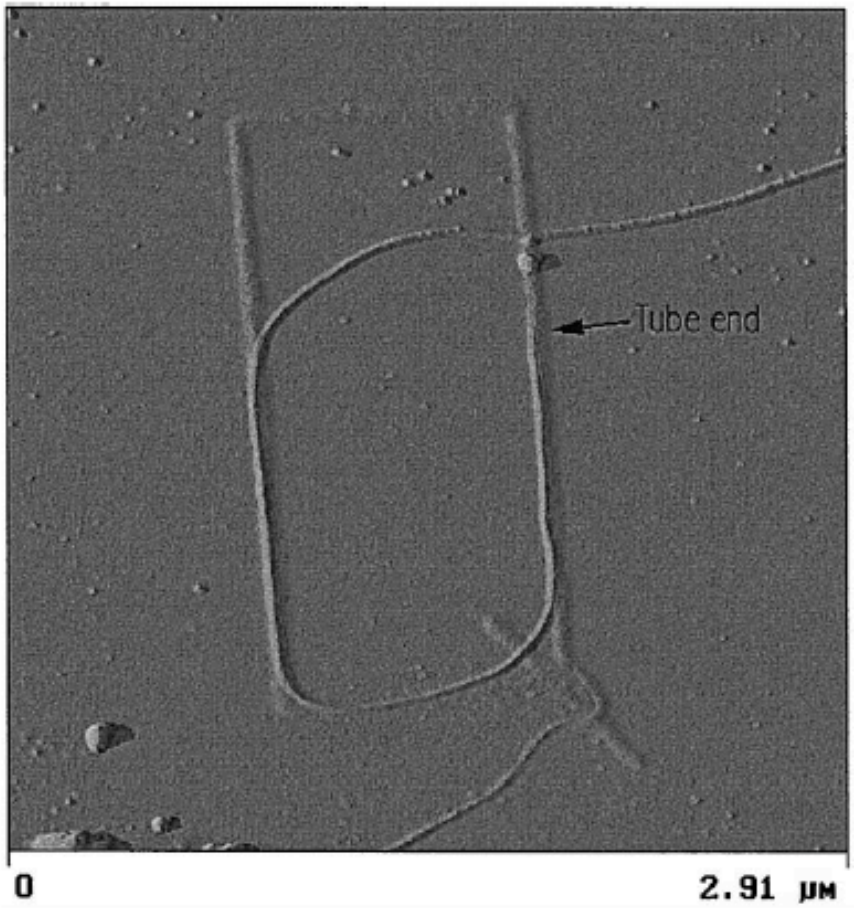

Fig. 4. Tapping mode AFM image of an individual SWNT aligning with chemically functionalized patterns on surface. Note the nanotube bends to align well with the pattern, which is an indication of strong interaction between the tube and $-NH_2$ on the surface.

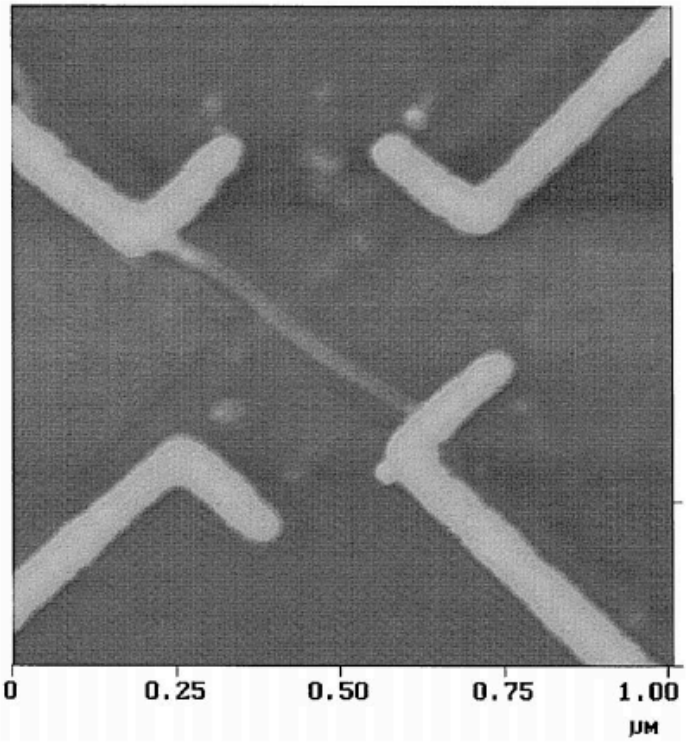

Fig. 5. Tapping mode AFM images of a device made of an individual SWNT connected to two Au electrodes.

Chemical Physics Letters 303 (1999) 125–129

CNT transistor

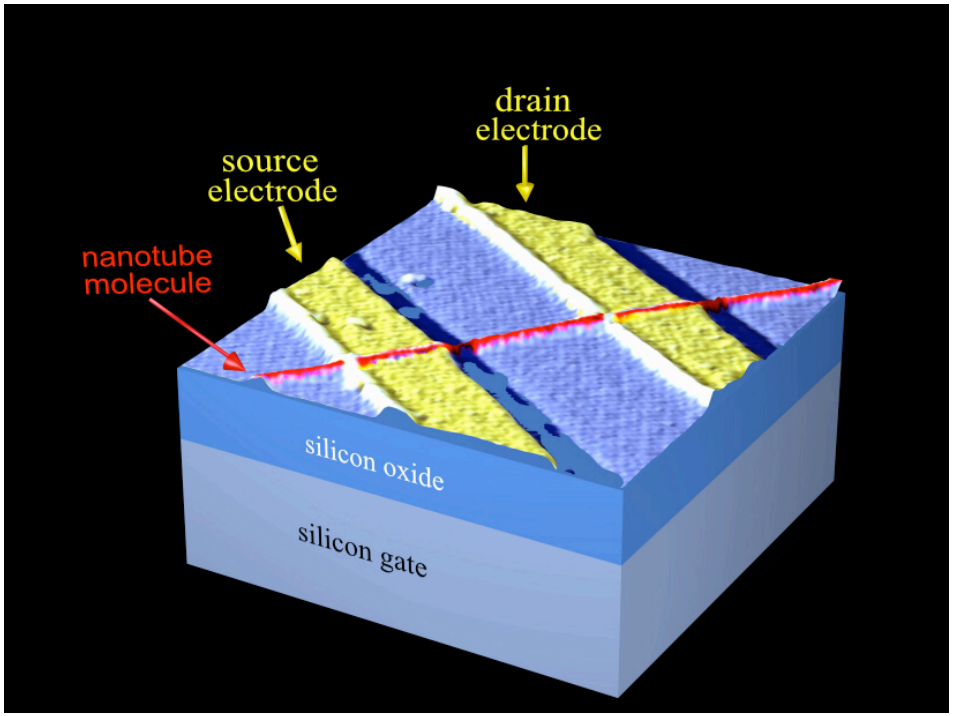

Room-temperature transistor based on a single carbon nanotube

Sander J. Tans, Alwin R. M. Verschueren & Cees Dekker

Department of Applied Physics and DIMES, Delft University of Technology, Lorentzweg 1, 2628 CJ Delft, The Netherlands

The use of individual molecules as functional electronic devices was first proposed in the 1970s (ref. 1). Since then, molecular electronics[2,3] has attracted much interest, particularly because it could lead to conceptually new miniaturization strategies in the electronics and computer industry. The realization of single-molecule devices has remained challenging, largely owing to difficulties in achieving electrical contact to individual molecules. Recent advances in nanotechnology, however, have resulted in electrical measurements on single molecules[4–7]. Here we report the fabrication of a field-effect transistor—a three-terminal switching device—that consists of one semiconducting[8–10] single-wall carbon nanotube[11,12] connected to two metal electrodes. By applying a voltage to a gate electrode, the nanotube can be switched from a conducting to an insulating state. We have previously reported[5] similar behaviour for a metallic single-wall carbon nanotube operated at extremely low temperatures. The present device, in contrast, operates at room temperature, thereby meeting an important requirement for potential practical applications. Electrical measurements on the nanotube transistor indicate that its operation characteristics can be qualitatively described by the semiclassical band-bending models currently used for traditional semiconductor devices. The fabrication of the three-terminal switching device at the level of a single molecule represents an important step towards molecular electronics.

NATURE | VOL 393 | 7 MAY 1998 49-52

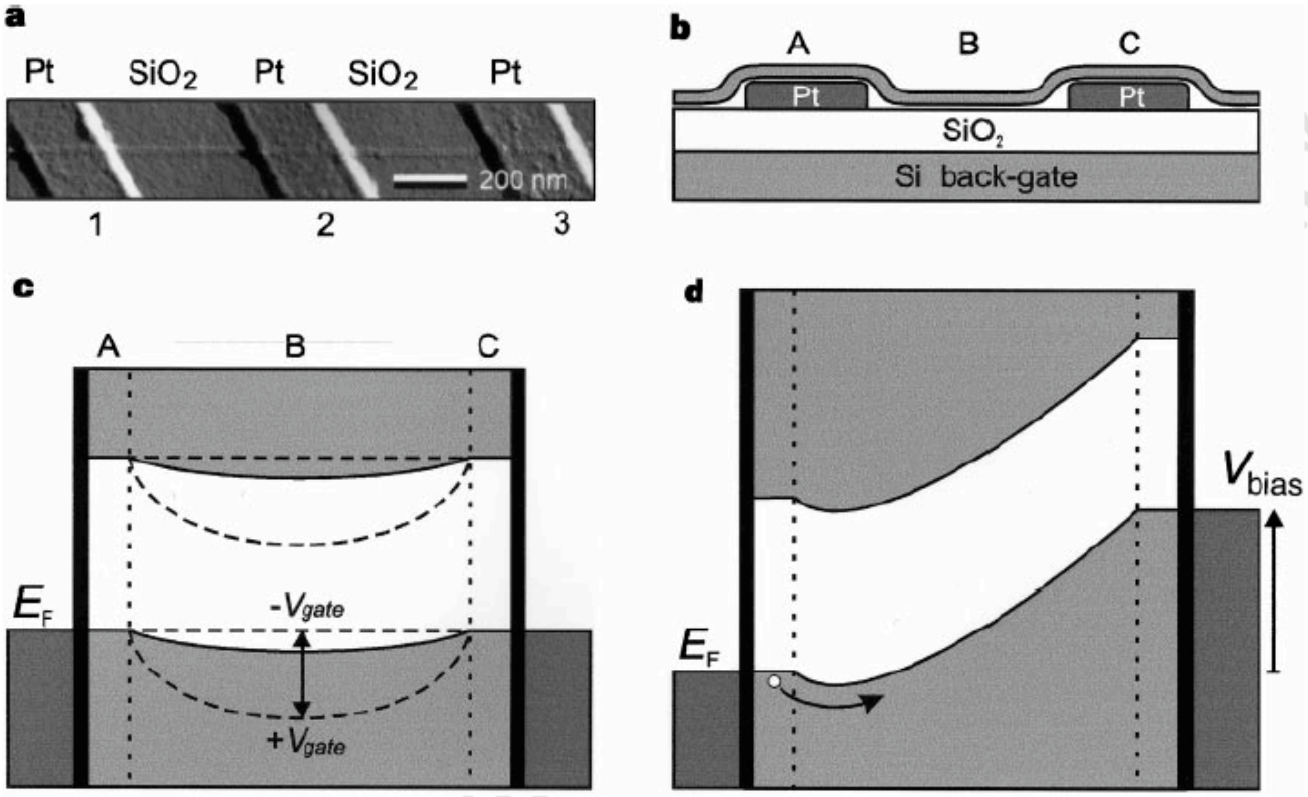

Figure 1 a, Tapping-mode AFM image of an individual carbon nanotube on top of three Pt electrodes. **b**, Schematic side view of the TUBEFET device. A single semiconducting nanotube is contacted by two electrodes. The Si substrate, which is covered by a layer of SiO_2 300 nm thick, acts as a back-gate. **c**, Suggested band diagram of the device. The nanotube with a gap of ~0.6 eV is connected to the leads with Fermi energy E_F by tunnelling contacts, indicated by the black vertical bars. At A and C (see **b**), the valence-band edge is pinned to the Fermi energy of the leads. Owing to a difference in work function between the tube and the electrodes, the bands bend towards lower energy in between the electrodes (B). For positive V_{gate} the bands bend more strongly, leading to an insulating state. For negative V_{gate} the bands flatten, resulting in a metal-like conductance. **d**, Application of a bias voltage results in a suppression of the barrier.

NATURE | VOL 393 | 7 MAY 1998 49-52

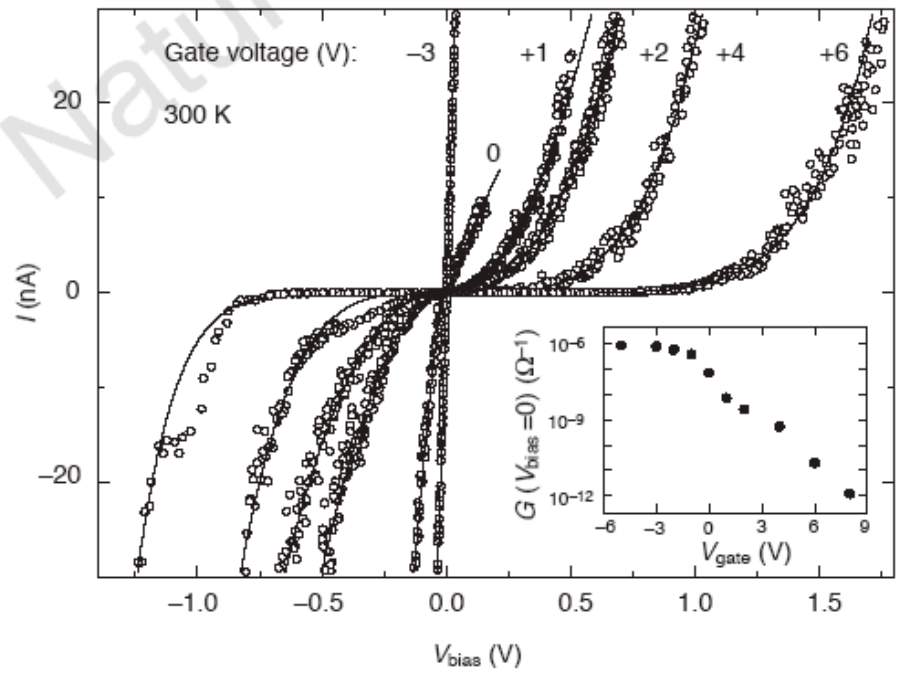

Figure 2 Two probe I–V_{bias} curves for various values of the gate voltage (V_{gate}). Data were taken at room temperature and in vacuum (~10^{-4} mbar), with the voltage applied to contacts 1 (drain) and 2 (source). A negative V_{gate} leads to ohmic behaviour while a positive V_{gate} results in a strong suppression of the current at low bias voltage and nonlinear I–V_{bias} curves at higher bias. Inset, conductance at $V_{bias} = 0$ as a function of V_{gate}. The conductance through this single molecular switch can be varied over at least six orders of magnitude and saturates at $10^{-6}\,\Omega^{-1}$ for negative V_{gate}.

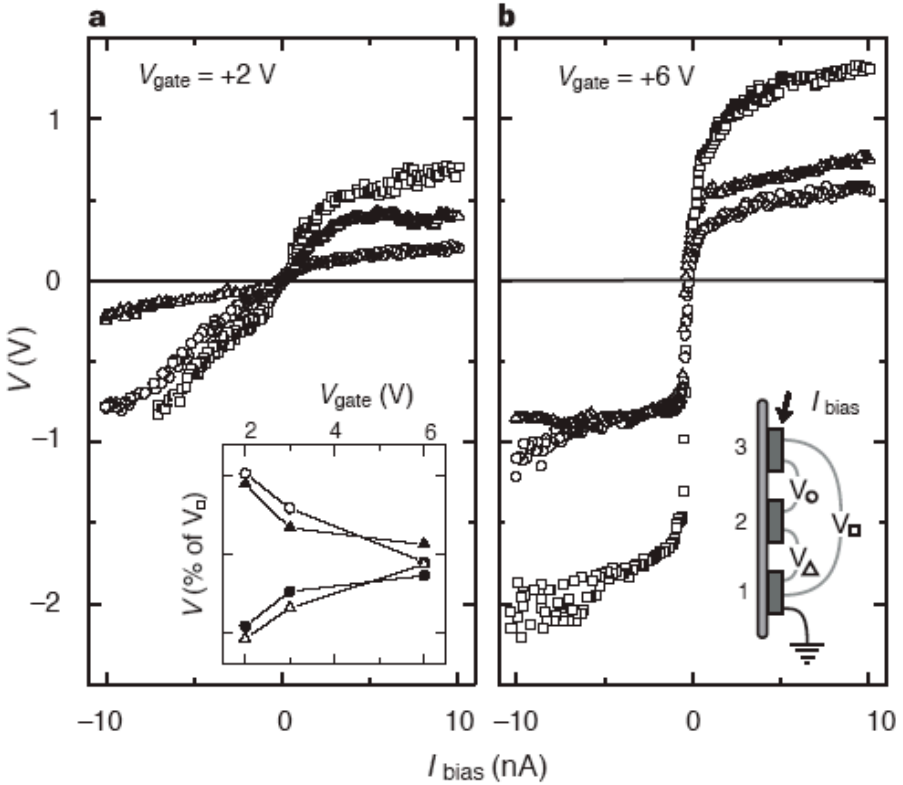

Figure 3 Three-probe I_{bias}–V curves for two gate voltages. The current is biased over the two outer contacts 1 and 3. The voltage drop is measured over contact pairs 1–2 (△), 2–3 (○) and 1–3 (□) (right inset). At low V_{gate} (**a**), the voltage drop over 1–2 is not the same as for 2–3, whereas for larger V_{gate} (**b**), the two voltages are identical. Left inset, voltages over pairs 1–2 and 2–3 as a percentage of the total voltage (1–3), both for negative bias (open symbols) and for positive bias (solid symbols). The observed behaviour is in agreement with the proposed band diagram of the device (Fig. 1).

NATURE | VOL 393 | 7 MAY 1998 49-52

CNT logic circuits

Logic Circuits with Carbon Nanotube Transistors

Adrian Bachtold,* Peter Hadley, Takeshi Nakanishi, Cees Dekker†

We demonstrate logic circuits with field-effect transistors based on single carbon nanotubes. Our device layout features local gates that provide excellent capacitive coupling between the gate and nanotube, enabling strong electrostatic doping of the nanotube from *p*-doping to *n*-doping and the study of the nonconventional long-range screening of charge along the one-dimensional nanotubes. The transistors show favorable device characteristics such as high gain (>10), a large on-off ratio (>10^5), and room-temperature operation. Importantly, the local-gate layout allows for integration of multiple devices on a single chip. Indeed, we demonstrate one-, two-, and three-transistor circuits that exhibit a range of digital logic operations, such as an inverter, a logic NOR, a static random-access memory cell, and an ac ring oscillator.

2001 VOL 294 SCIENCE 1317-1320

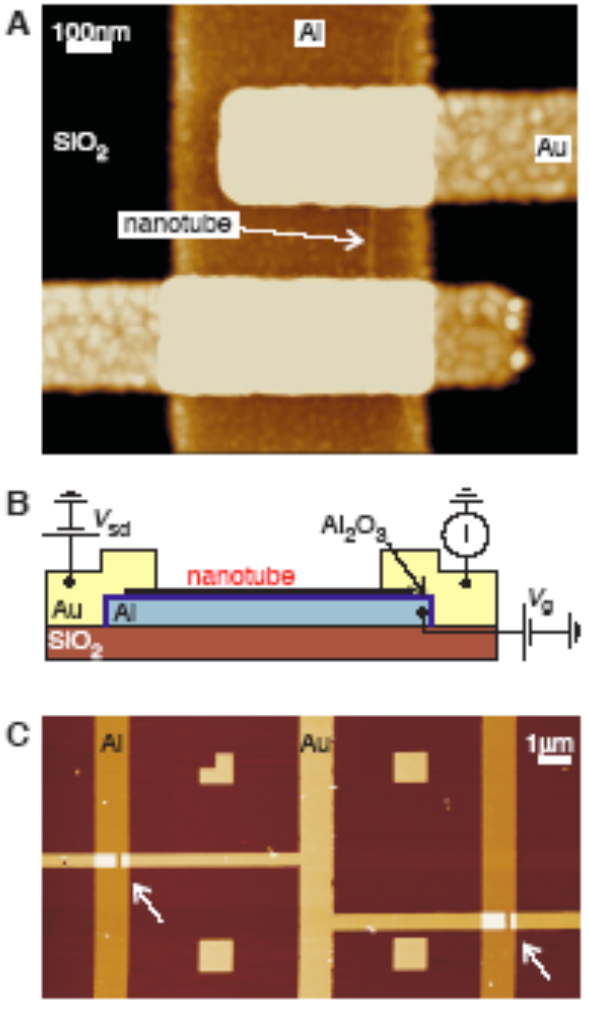

Fig. 1. Device layout. (**A**) Height image of a single-nanotube transistor, acquired with an atomic force microscope. (**B**) Schematic side view of the device. A semiconducting nanotube is contacted by two Au electrodes. An Al wire, covered by a few-nanometers-thick oxide layer, is used as a gate. (**C**) Height-mode atomic force microscope image of two nanotube transistors connected by a Au interconnect wire. The arrows indicate the position of the transistors. Four alignment markers can also be seen.

CNT logic circuits 2

Fig. 4. Demonstration of one-, two-, and three-transistor logic circuits with carbon nanotube FETs. (A) Output voltage as a function of the input voltage of a nanotube inverter. (Inset) Schematic of the electronic circuit. The resistance is 100 megaohms. (B) Output voltage of a nanotubes NOR for the four possible input states (1,1), (1,0), (0,1), and (0,0). A voltage of 0 V represents a logical 0 and a voltage of −1.5 V represents a logical 1. The resistance is 50 megaohms. (C) Output voltage of a flip-flop memory cell (SRAM) composed of two nanotube FETs. The output logical stays at 0 or 1 after the switch to the input has been opened. The two resistances are 100 megaohms and 2 gigaohms. (D) Output voltage as a function of time for a nanotube ring oscillator. The three resistances are 100 megaohms, 100 megaohms, and 2 gigaohms.

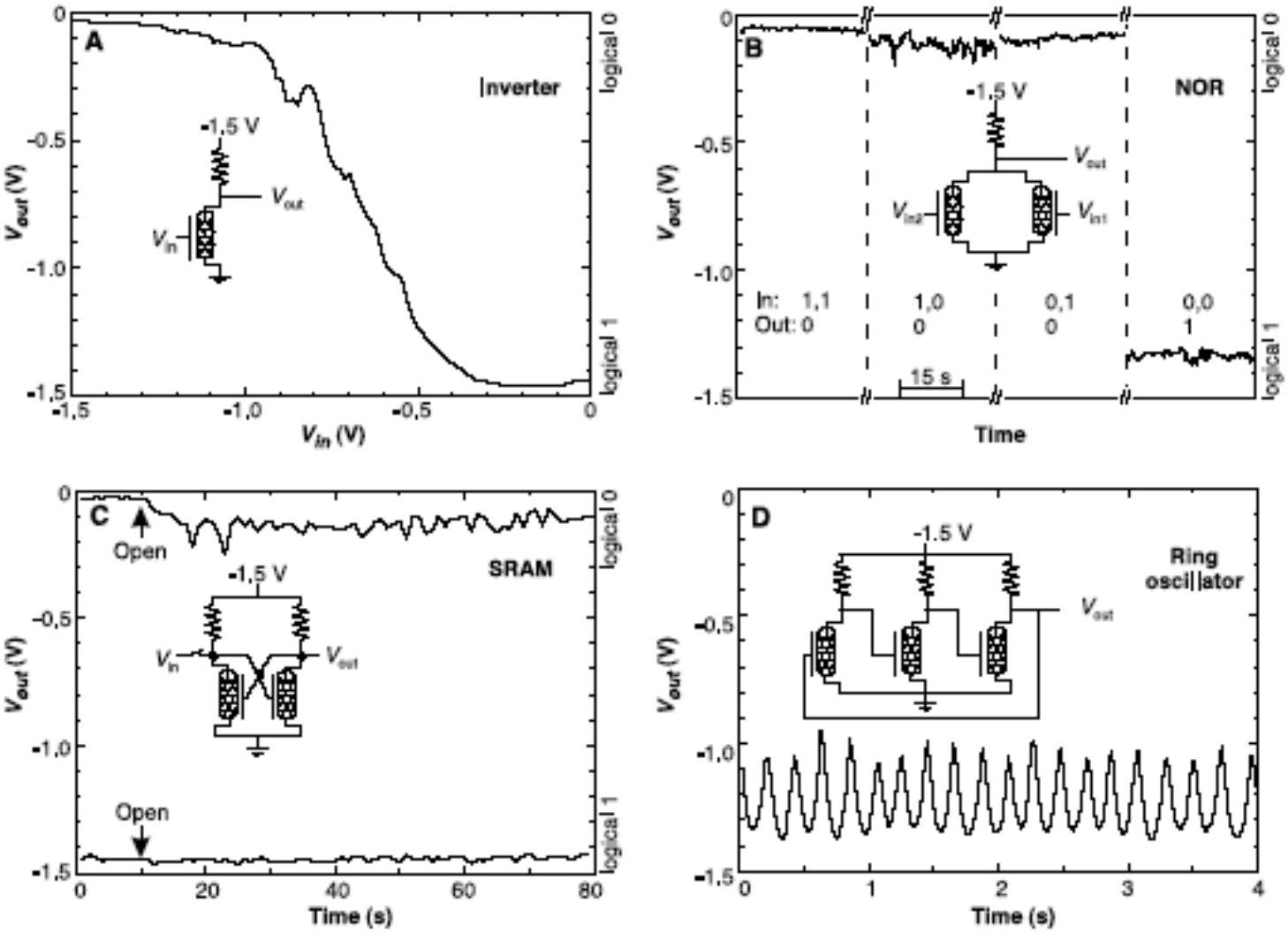

2001 VOL 294 SCIENCE 1317-1320

Crossed Nanotube Junctions

M. S. Fuhrer,[1] J. Nygård,[1] L. Shih,[1] M. Forero,[1] Young-Gui Yoon,[1]
M. S. C. Mazzoni,[1] Hyoung Joon Choi,[2] Jisoon Ihm,[2]
Steven G. Louie,[1] A. Zettl,[1] Paul L. McEuen[1]*

Junctions consisting of two crossed single-walled carbon nanotubes were fabricated with electrical contacts at each end of each nanotube. The individual nanotubes were identified as metallic (M) or semiconducting (S), based on their two-terminal conductances; MM, MS, and SS four-terminal devices were studied. The MM and SS junctions had high conductances, on the order of 0.1 e^2/h (where e is the electron charge and h is Planck's constant). For an MS junction, the semiconducting nanotube was depleted at the junction by the metallic nanotube, forming a rectifying Schottky barrier. We used two- and three-terminal experiments to fully characterize this junction.

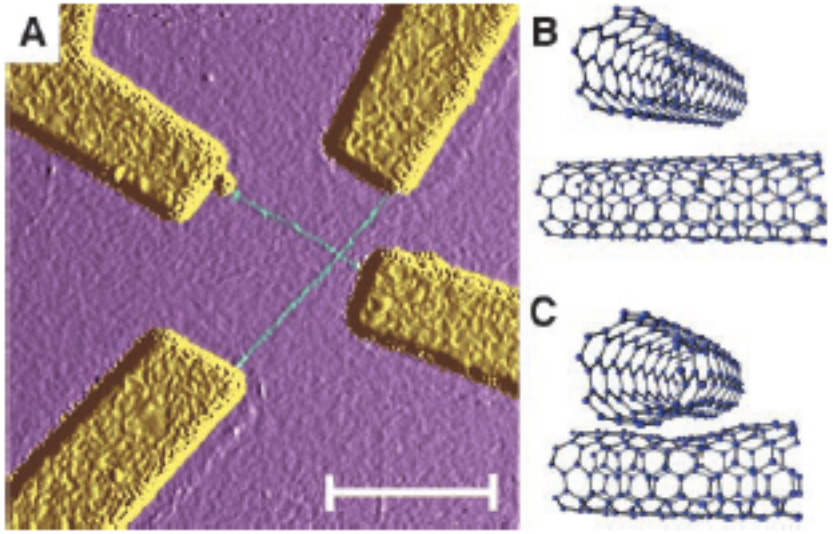

Fig. 1. (A) Tapping-mode AFM image (amplitude signal) of a crossed SWNT device. Two SWNTs (green) can be seen spanning between the Cr/Au electrodes (yellow). (B and C) The structures used to calculate the conductance of a junction between two metallic (5,5) SWNTs (see text and supplementary material).

2000 VOL 288 SCIENCE 494-497

Crossed CNT junctions

2000 VOL 288 SCIENCE 494-497

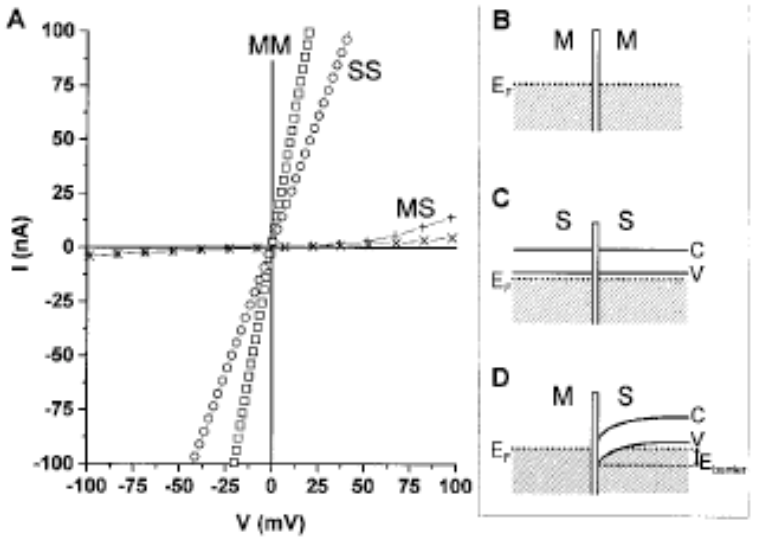

Fig. 2. (A) *I-V* characteristics of several SWNT junctions. Open squares, four-terminal measurement of an MM at 200 K; open circles, two-terminal measurement of an SS at 200 K; crosses and plus signs, two-terminal measurements of MS junctions at 50 K and $V_g = -25V$. (B through D) The expected band structures near the junctions. There exists a finite density of states on either side of the junction for (B) the MM and (C) the SS junctions. (D) In the MS junction, a Schottky barrier of height $E_{barrier}$ forms in the semiconducting SWNT because of charge transfer from the metallic SWNT. (The conduction and valence bands of the semiconducting SWNTs are denoted by *C* and *V* and the Fermi level by E_F).

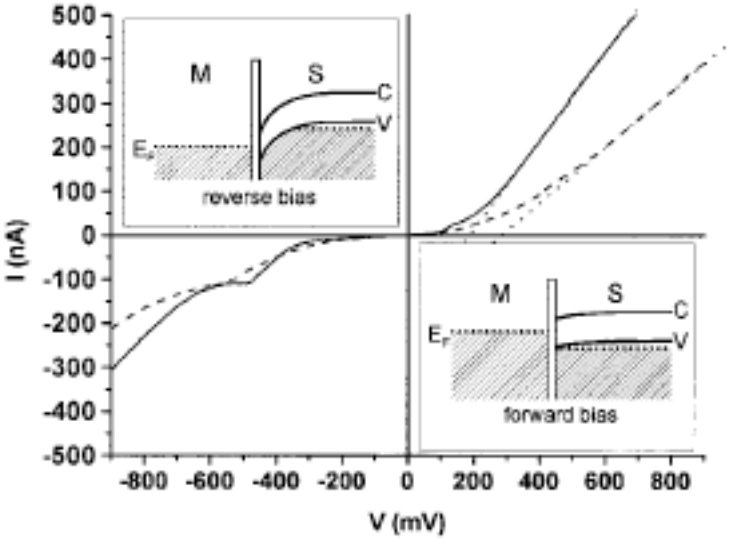

Fig. 3. Two-terminal *I-V* characteristics of two metallic SWNT–semiconducting SWNT junctions at a temperature of 50 K (solid and dashed lines). Bias was applied to the semiconducting SWNT. The dotted lines are linear fits to the forward bias data. The schematic energy level diagrams for the reverse bias (upper left inset) and forward bias (lower right inset) are shown.

Reversible water-solubilization of single-walled carbon nanotubes by polymer wrapping

Michael J. O'Connell, Peter Boul, Lars M. Ericson, Chad Huffman, Yuhuang Wang, Erik Haroz, Cynthia Kuper, Jim Tour, Kevin D. Ausman, Richard E. Smalley *

Department of Chemistry and Center for Nanoscale Science and Technology, Rice University, MS-60, P.O. Box 1892, Houston, TX 77251-1892, USA

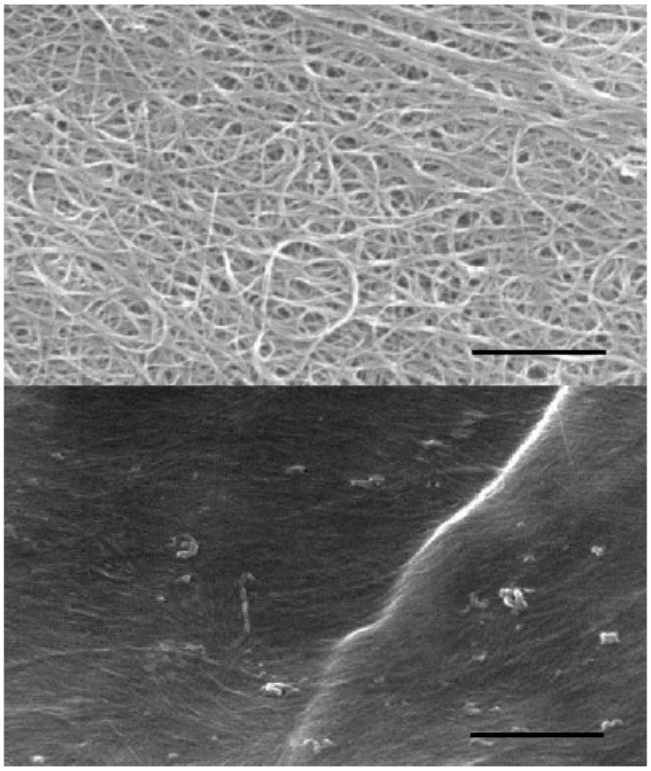

Fig. 2. Typical paper formed by filtering SWNTs from organic or surfactant suspension, consisting of large ropes (top). Paper formed by filtering PVP–SWNTs (bottom). Scale bars are 500 nm.

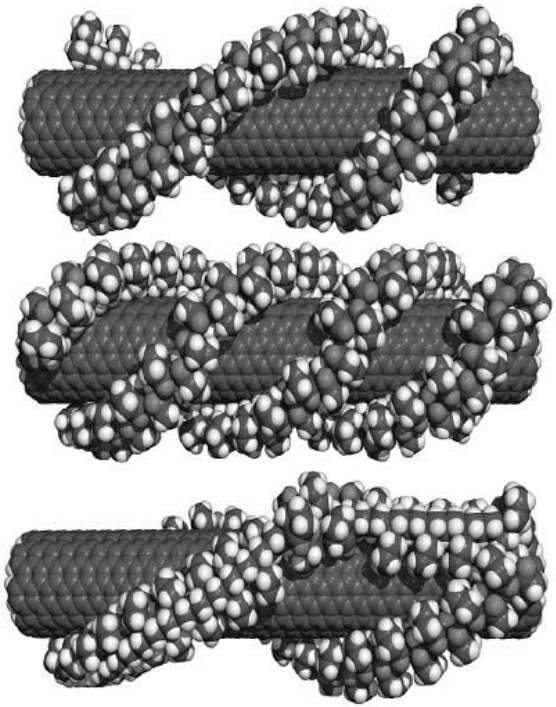

Fig. 4. Some possible wrapping arrangements of PVP on an 8,8 SWNT. A double helix (top) and a triple helix (middle). Backbone bond rotations can induce switch-backs, allowing multiple parallel wrapping strands to come from the same polymer chain (bottom).

polyvinyl pyrrolidone (PVP) and polystyrene sulfonate (PSS)

Chemical Physics Letters 342 (2001) 265–271

Nanotechnology 13 (2002) 601–604 PII: S0957-4484(02)40069-4

DNA-functionalized single-walled carbon nanotubes

Chris Dwyer[1], Martin Guthold[2], Michael Falvo[2], Sean Washburn[2], Richard Superfine[2] and Dorothy Erie[3]

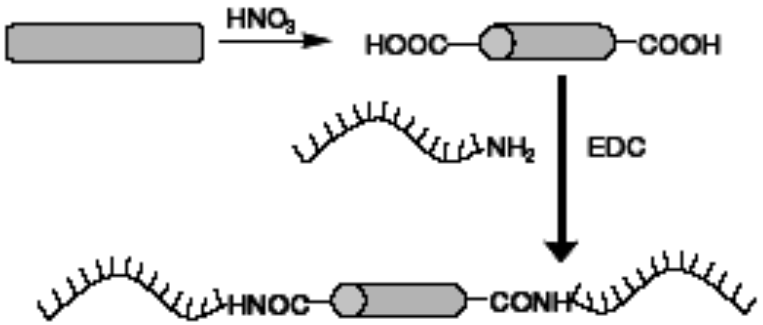

Figure 1. The DNA/nanotube reaction scheme. Capped nanotubes are oxidatively opened and then reacted with amine-terminated single-stranded DNA.

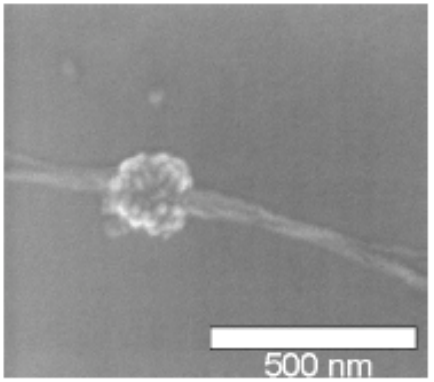

Figure 4. A lambda-DNA cluster attached to defect sites and ends of a SWNT bundle.

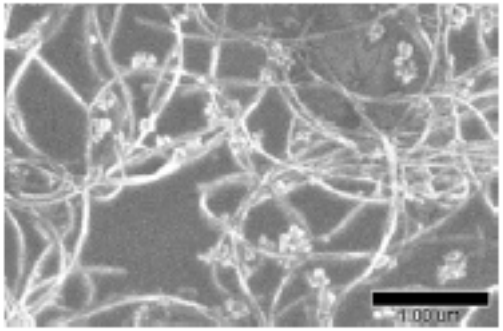

Figure 5. Lambda-DNA clusters on SWNT bundles.

DNA on CNT (adsorb)

Structure-Based Carbon Nanotube Sorting by Sequence-Dependent DNA Assembly

Ming Zheng,[1]* Anand Jagota,[1] Michael S. Strano,[2] Adelina P. Santos,[3]† Paul Barone,[2] S. Grace Chou,[3] Bruce A. Diner,[1] Mildred S. Dresselhaus,[3] Robert S. Mclean,[1] G. Bibiana Onoa,[1] Georgii G. Samsonidze,[3] Ellen D. Semke,[1] Monica Usrey,[2] Dennis J. Walls[1]

Wrapping of carbon nanotubes (CNTs) by single-stranded DNA (ssDNA) was found to be sequence-dependent. A systematic search of the ssDNA library selected a sequence d(GT)n, n = 10 to 45 that self-assembles into a helical structure around individual nanotubes in such a way that the electrostatics of the DNA-CNT hybrid depends on tube diameter and electronic properties, enabling nanotube separation by anion exchange chromatography. Optical absorption and Raman spectroscopy show that early fractions are enriched in the smaller diameter and metallic tubes, whereas late fractions are enriched in the larger diameter and semiconducting tubes.

SCIENCE VOL 302 28 NOVEMBER 2003 1545-1548

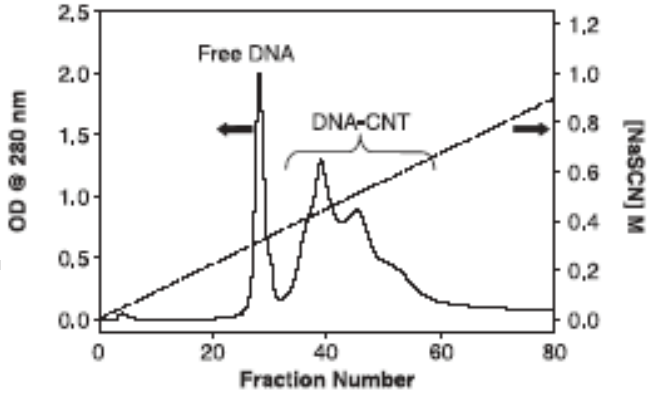

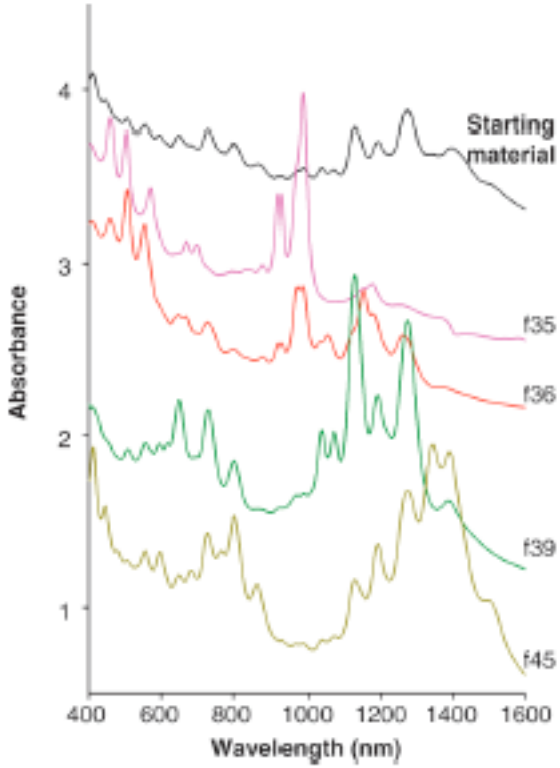

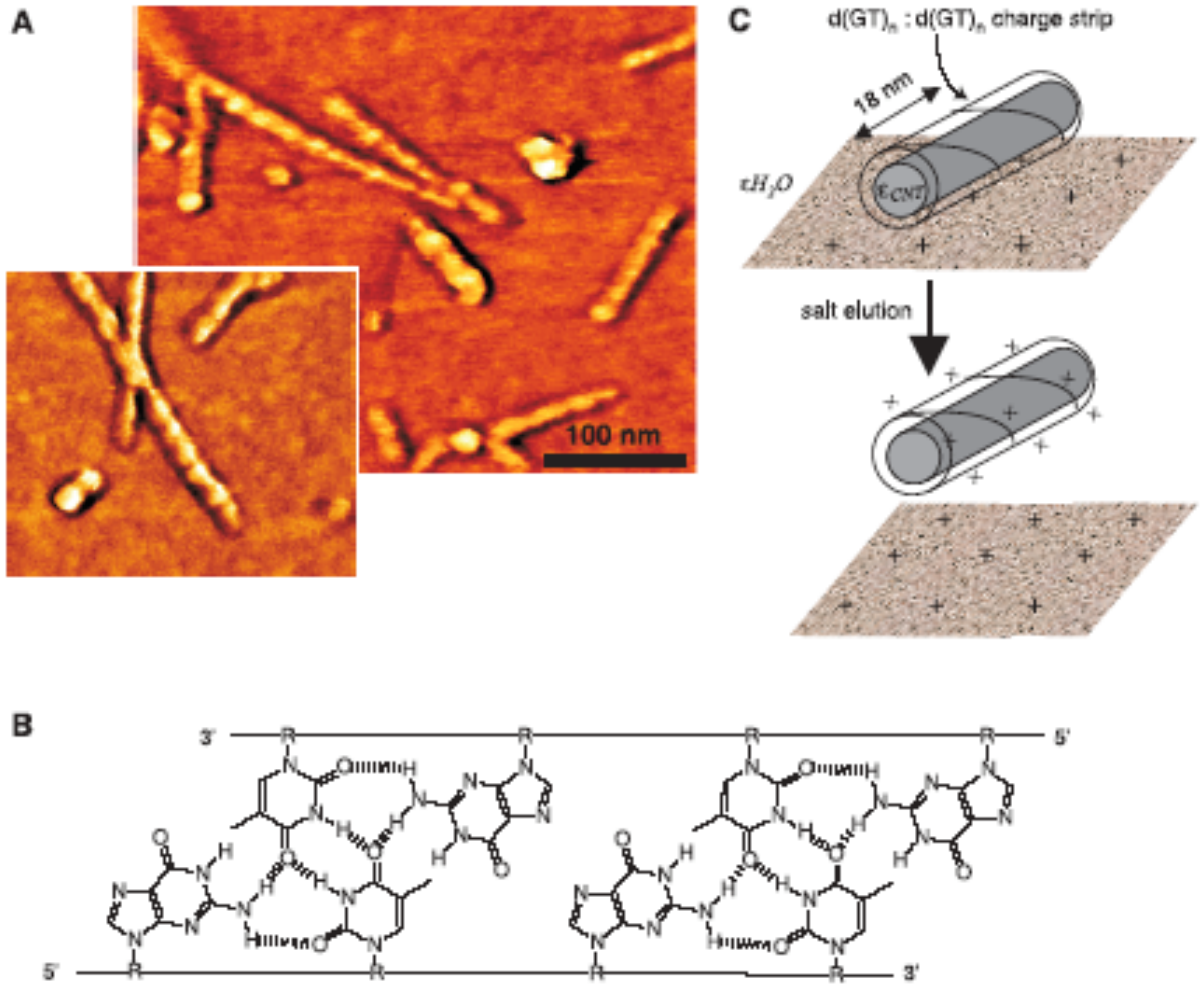

Fig. 4. Mechanism of DNA-CNT separation. (A) AFM (phase image) of CNTs wrapped by d(GT)30, showing regular helical pitch of ~18 nm and height of ~2 nm. (B) Proposed hydrogen-bonding interactions between two d(GT)n strands that lead to the formation of a "d(GT)n:d(GT)n charge strip." (C) Schematic for anion exchange separation process. At lower salt concentration, the surface-bound state is favored in which positive ions on the resin attract the negative surface charge on the DNA-CNT. With increasing salt concentration, the surface and DNA-CNT interactions are screened, favoring elution.

SCIENCE VOL 302 28 NOVEMBER 2003 1545-1548

DNA-assisted dispersion and separation of carbon nanotubes

MING ZHENG*, ANAND JAGOTA, ELLEN D. SEMKE, BRUCE A. DINER, ROBERT S. MCLEAN, STEVE R. LUSTIG, RAYMOND E. RICHARDSON AND NANCY G. TASSI

DuPont Central Research and Development, Experimental Station, Wilmington, Delaware 19880, USA

nature materials | VOL 2 | MAY 2003 | 338-342

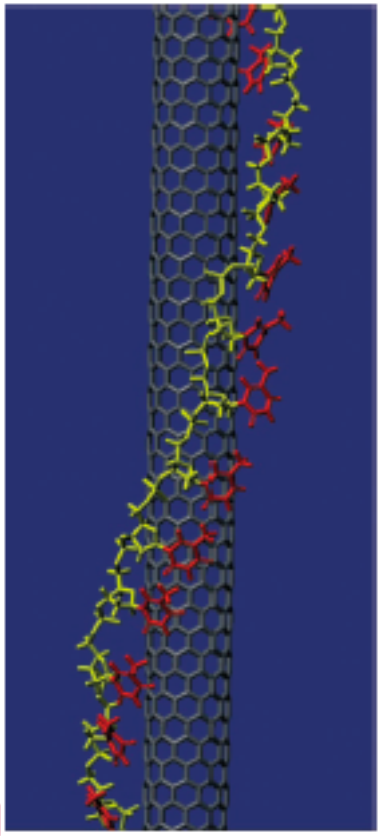

- NA: poly-T, in vitro evolved ssDNA, dsDNA or RNA from bacteria or yeast.
- NA+surfactant+sonication.
- Near-IR fluorescence indicates well dispersed SWNT.
- Anion-exchange chromatography separates DNA-CNT by size and electronic tube-type.

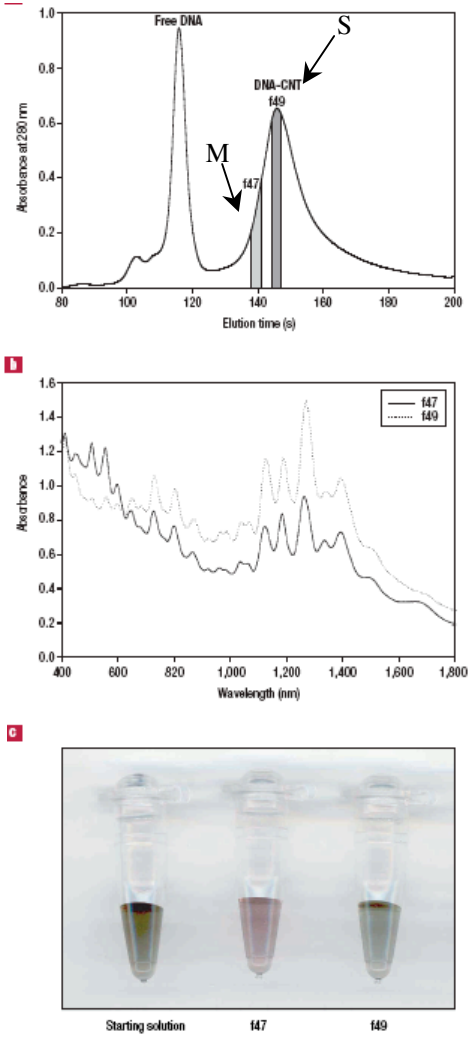

Figure 3 Separation of DNA-CNT by anion exchange chromatography. a, Chromatogram of anion-exchange column separation of (C/T)60 dispersed carbon nanotubes, showing the two different bands due to free DNA and DNA-CNT. The position of fractions 47 (f47) and 49 (f49) are shown. b, Electronic absorption spectra of two fractions f47 and f49. Before the measurement, fractions were centrifuged using a microcon spin filter YM100 (Millipore), and re-suspended in 0.1 M sodium chloride D_2O solution with an appropriate volume to concentrate f47 by fivefold, and f49 by 1.67-fold. c, Visual comparison of DNA-CNT solutions of the starting material, f47 and f49.

Functionalization of Carbon Nanotubes for Biocompatibility and Biomolecular Recognition

Moonsub Shim, Nadine Wong Shi Kam, Robert J. Chen, Yiming Li, and Hongjie Dai*

Department of Chemistry, Stanford University, Stanford, California 94305

NANO LETTERS

2002
Vol. 2, No. 4
285–288

- Non-specific binding of protein to CNT.
- Inhibition by PEG coating.
- Specific protein binding enabled.

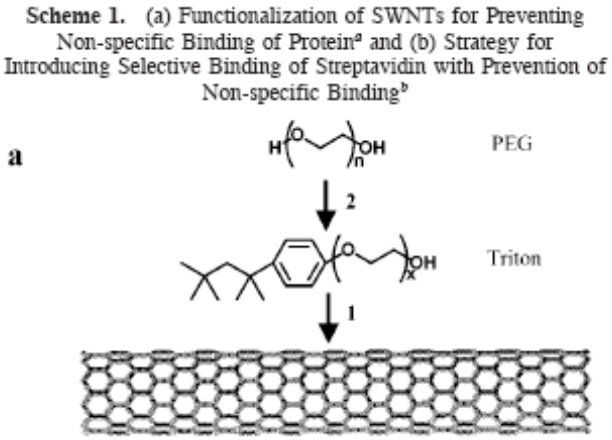

Scheme 1. (a) Functionalization of SWNTs for Preventing Non-specific Binding of Protein[a] and (b) Strategy for Introducing Selective Binding of Streptavidin with Prevention of Non-specific Binding[b]

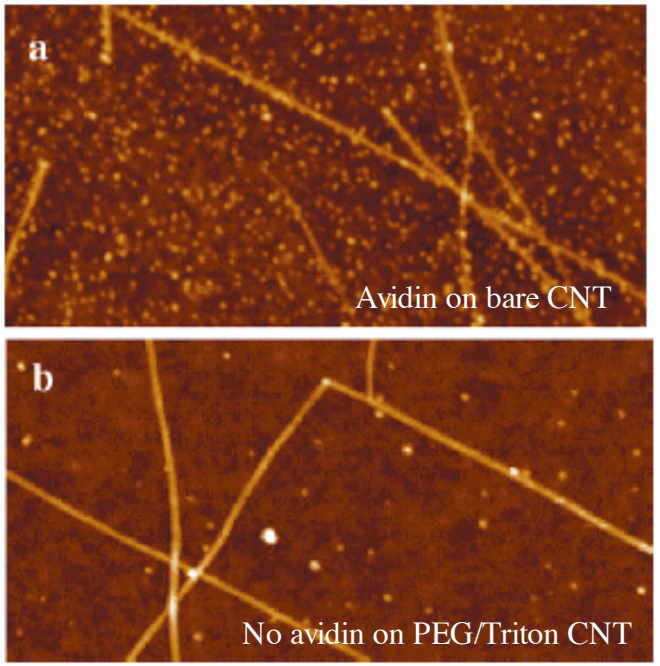

Figure 1. (a) AFM image of streptavidin (dots along the SWNTs) adsorbed nonspecifically on as-grown SWNTs (line-like features). The diameters (topographic heights) of SWNTs shown in all of the Figures are 1 to 3 nm. (b) AFM image showing nonspecific streptavidin binding is prevented by coating SWNTs with a surfactant, Triton X-100, and a well-known protein resistant polymer PEG (Scheme 1a). Both images are 0.5 × 1 μm.

NANO LETTERS
2002
Vol. 2, No. 4
285−288

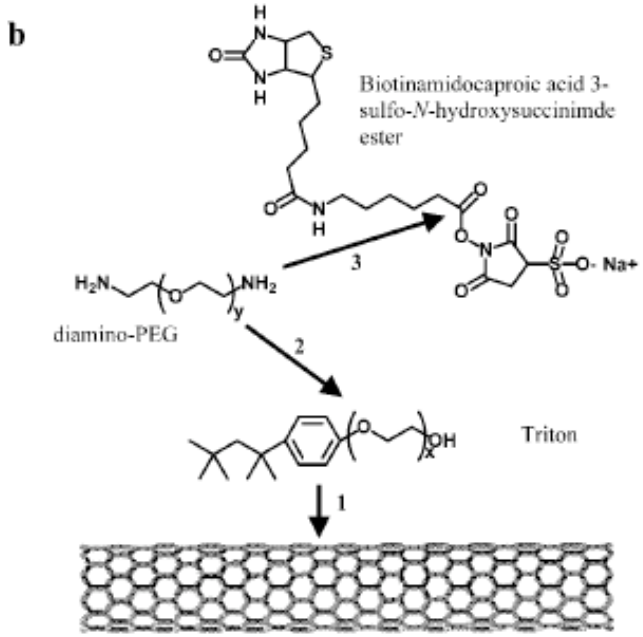

[a] A surfactant Triton-X 100 is first adsorbed onto the sidewalls of SWNTs followed by adsorption of PEG. [b] Triton-X 405 is adsorbed on SWNTs followed by amine-terminated PEG covalently linked to biotin.

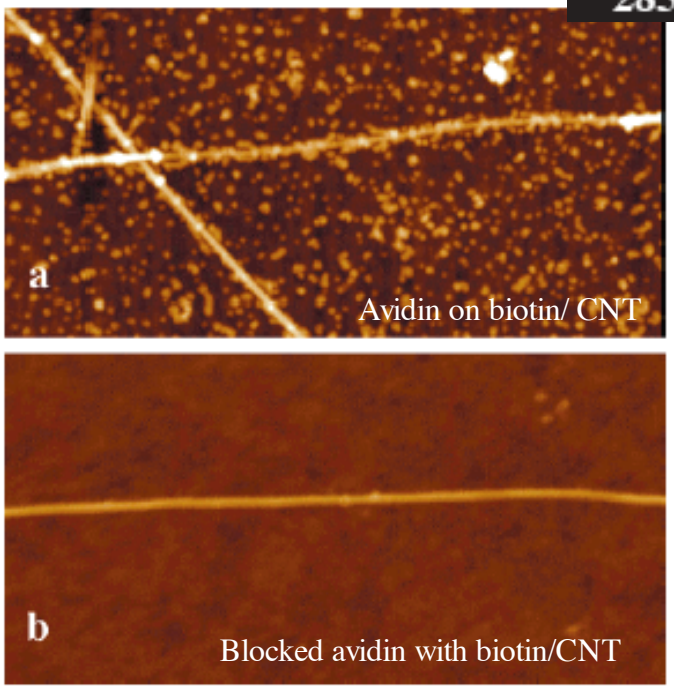

Figure 2. (a) AFM image showing specific adsorption of streptavidin by co-functionalization of SWNTs with a protein repelling layer and biotin (Scheme 1b). SWNTs are first coated with surfactant Triton X-405 then by diamino-PEG followed by covalent linkage of succinimidyl ester terminated biotin to the amine moieties of the PEG. (b) Control experiment where SWNTs are co-functionalized with PEG and biotin as in (a) but exposed to streptavidin that has been plugged with biotin prior to adsorption onto SWNTs. Images are 0.5 × 1 μm.

- Anything curious about this data?

Noncovalent functionalization of carbon nanotubes for highly specific electronic biosensors

Robert J. Chen*, Sarunya Bangsaruntip*, Katerina A. Drouvalakis†, Nadine Wong Shi Kam*, Moonsub Shim*, Yiming Li*, Woong Kim*, Paul J. Utz†, and Hongjie Dai*‡

*Department of Chemistry, and †School of Medicine, Department of Medicine, Division of Immunology and Rheumatology, Stanford University, Stanford, CA 94305

4984–4989 | PNAS | April 29, 2003 | vol. 100 | no. 9

- Non-specific binding of proteins to CNT.
- Inhibition by PEO coating.
- Construction of specific biosensors by coating with PEO-conjugates.
- Quartz crystal microbalance (QCM) and direct electrical measurements.

(Non-ionic surfactants)

Table 1. Survey of whether various proteins bind to as-grown nanotubes and nanotubes treated with the listed molecules

Nanotubes	SA	Avidin	BSA	GCD	SpA
As-grown nanotubes	Y	Y	Y	Y	Y
Tween 20-treated	N	N	N	N	N
Pluronic P103-treated	N	N	N	N	N
Triton X-100-treated	N	Y	Y	Y	N
Dextran-treated	Y	Y	Y	Y	Y

N indicates no binding and thus effective protein resistance. Y indicates NSB of proteins and thus poor or no protein resistance. GCD, α-glucosidase.

QCM

Quartz crystal microbalance.

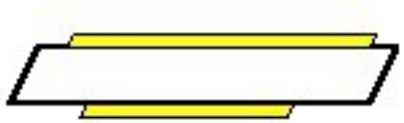

AT-cut piezoelectric quartz microbalance: A quartz disk ~1 cm in diameter and ~.1 mm thick with circular gold electrodes in the center of each face. When an A.C. voltage is applied across the electrodes the crystal oscillates in a thickness shear mode in which the two faces move parallel to each other and in opposite directions.

Used in this way the quartz becomes a mechanical resonator. Any adsorbed film on the electrodes will make the resonator heavier and so lower it's resonant frequency. A film thickness measurement is made by monitoring this frequency shift. The crystals used for these experiments were usually driven at their third harmonic ($\mathbf{f}_{o,3}$ ~ 5.5 MHz).

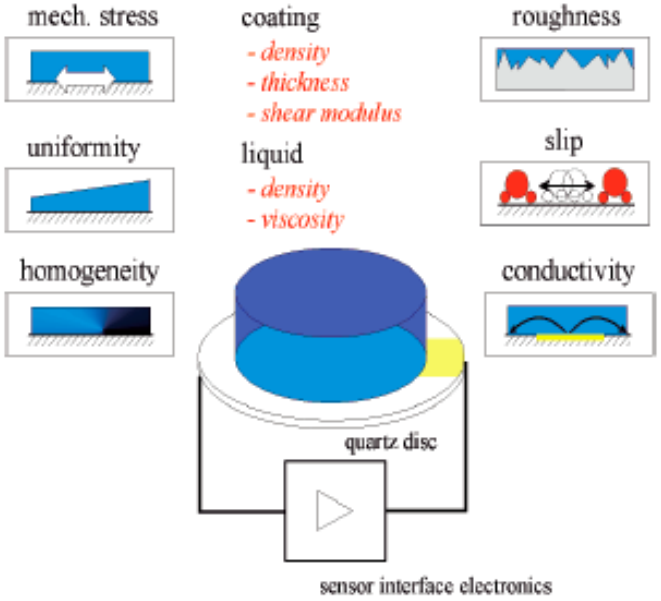

Influences on the behaviour of quartz crystals

4984–4989 | PNAS | April 29, 2003 | vol. 100 | no. 9

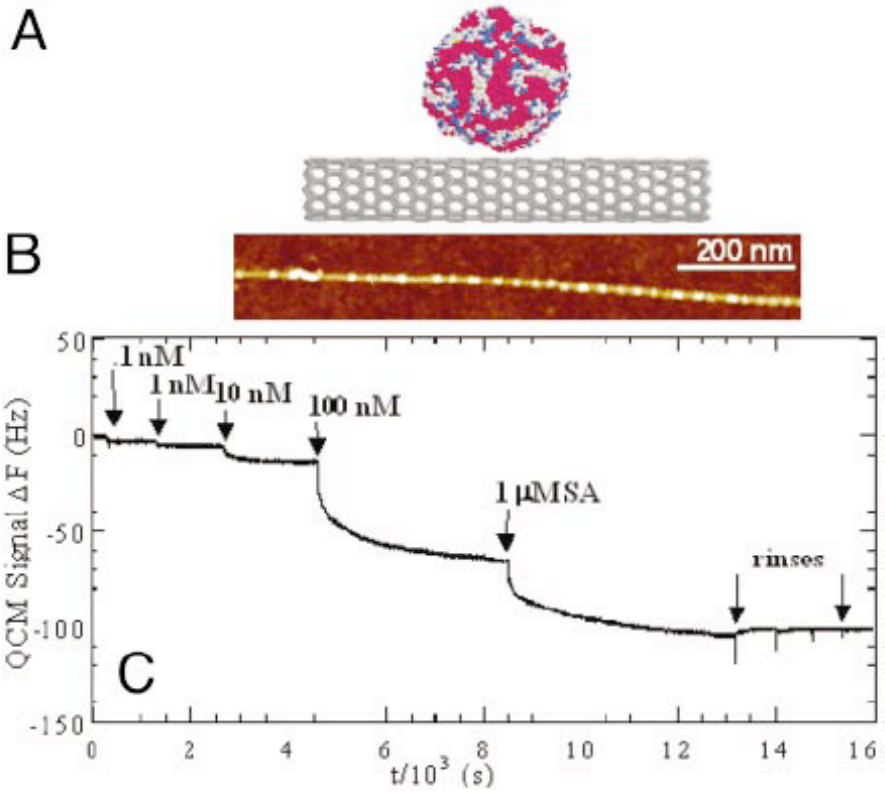

Fig. 1. Proteins tend to bind nonspecifically onto as-grown carbon nanotubes. (*A*) Schematic illustration of globular protein adsorption onto a nanotube. (*B*) An AFM image showing protein A (bright dot-like structures decorating the line-like nanotube) nonspecifically adsorbed on a nanotube. We have also observed a certain degree of NSB of proteins on regions of the (SiO_2) substrate free of nanotubes (data not shown). (*C*) QCM data (frequency shift ΔF vs. time t) revealing NSB of SA onto nanotubes at increasing protein concentrations. The NSB is irreversible upon rinsing.

Nanotube Electronic Devices for Sensing in Solution. Devices (see Fig. 2*A*) were prepared by nanotube synthesis on 1-cm × 2-cm quartz substrates. Twenty to 50 μl of a ferritin solution (6.9 mg/ml) was deposited as a rectangular strip (1–2 mm × 10 mm) on the substrate, allowed to dry, and then calcined in air at 800°C for 5 min. The resulting discrete iron nanoparticles act as catalytic seeds for nanotube growth during subsequent chemical vapor deposition of methane to afford a layer of interconnected SWNTs (15). Metal evaporation through a shadow mask formed the final device, SWNTs bridging two Ti/Au (20/60 nm thick, electrode spacing ≈0.5–1 mm) electrodes. Sensing in solution (see Fig. 2) was carried out by monitoring electrical current through the SWNT device (resistance on the order of kiloohms) under a 10-mV bias during protein additions in 10 mM phosphate buffer solution (pH 7.0). At this low bias, control experiments revealed no appreciable ionic current through the solution.

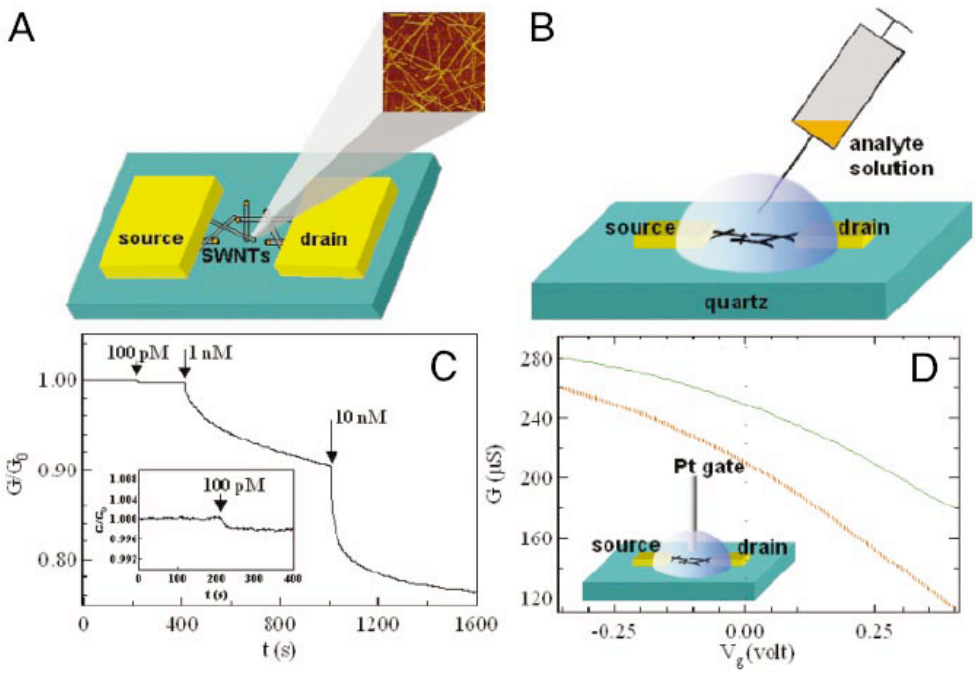

Fig. 2. Carbon nanotubes as electronic devices for sensing in aqueous solutions. (*A*) Schematic views of the electronic sensing device consisting of interconnected nanotubes bridging two metal electrode pads. An AFM image of a portion of the nanotube network (0.5 μm on a side) is shown. (*B*) Schematic setup for sensing in solution. (*C*) Conductance (G) evolution of a device for electronic monitoring of SA adsorption on nanotubes. The conductance is normalized by the initial conductance G_0. (*Inset*) Sensitivity to a 100-pM protein solution is shown. (*D*) Electrical conductance (G) vs. gate voltage (V_g) for a device in a 10-mM phosphate buffer solution. The gate voltage is applied through a Pt electrode immersed in the solution (*Inset*). The green (solid) and orange (broken) curves are the G–V_g characteristics for the device before and after SA binding, respectively. The shift in the two curves suggests a change in the charge environment of the nanotubes.

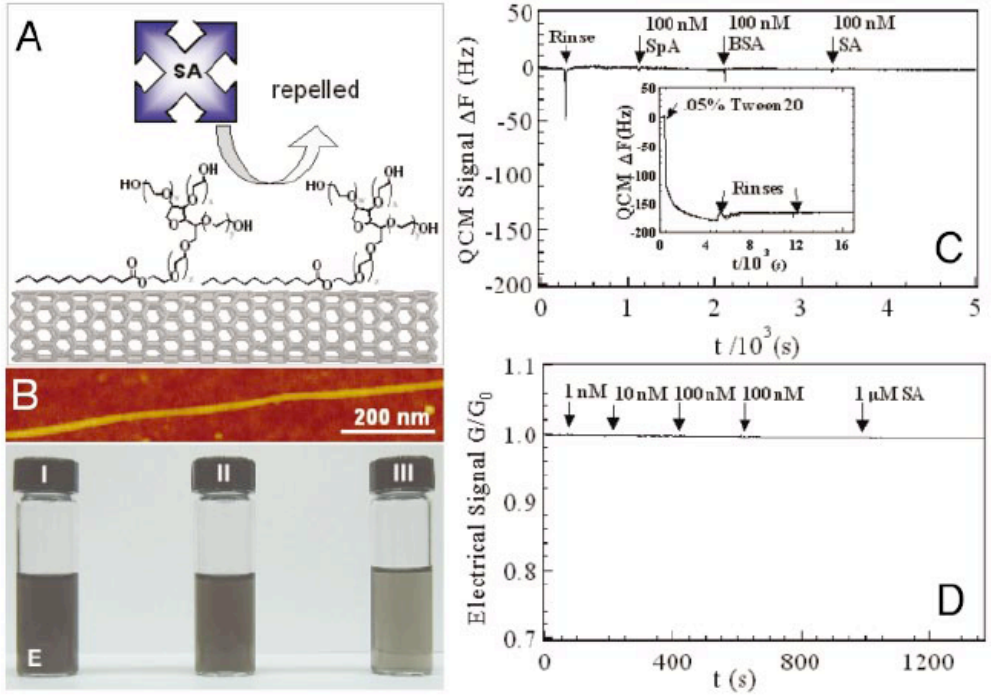

Fig. 3. Noncovalent functionalization of nanotubes for protein resistance and water solubility. (*A*) Schematic of a monolayer of Tween 20 anchored on a nanotube, repelling NSB of proteins in solution. (*B*) An AFM image showing the absence of adsorbed proteins on a Tween-coated nanotube after exposure to a 10-nM SA solution for 60 min. (*C*) QCM data showing the absence of mass uptake and thus no NSB of various proteins onto a film of Tween-coated nanotubes. (*Inset*) The irreversible adsorption of Tween onto such a film is shown. (*D*) The conductance of a Tween-coated nanotube electronic device does not exhibit any change upon exposure to various protein solutions. (*E*) Photographs that show SWNTs coated with Tween (I) and P103 (II) forming stable suspensions in water. The suspension in III is derived from $C_{14}E_8$-treated SWNTs, but to obtain a stable suspension, a lower concentration of SWNTs is necessary, resulting in a lighter-color solution than those in I and II.

4984–4989 | PNAS | April 29, 2003 | vol. 100 | no. 9

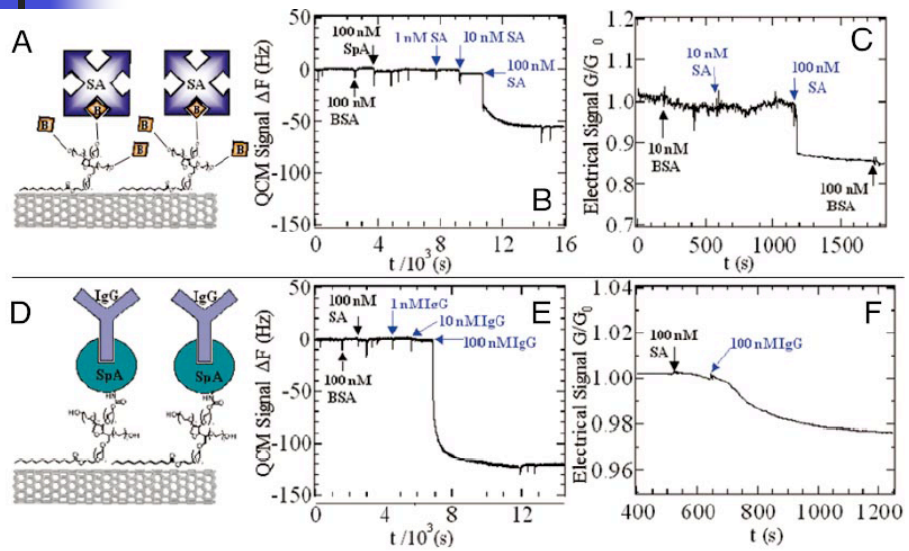

Fig. 4. Real-time QCM and electronic sensing of specific biological recognition on nanotubes. (*A*) Scheme for SA recognition with a nanotube coated with biotinylated Tween. (*B*) QCM frequency shift vs. time curve showing that a film of nanotubes coated with biotinylated Tween binds SA specifically but not other proteins. (*C*) Conductance vs. time curve of a device during exposure to various protein solutions. Specific binding of SA is detected electronically. (*D*) Scheme for IgG recognition with a nanotube coated with a SpA–Tween conjugate. (*E*) QCM frequency shift vs. time curve showing a film of nanotubes coated with SpA–Tween binding human IgG specifically but not unrelated proteins. Note that 10 nM IgG concentration approaches the lower detection limit of the instrument, whereas 100 nM approaches surface saturation of the sample; thus, the response does not show a full proportionality to the concentration. (*F*) Conductance vs. time curve of a device during exposure to various protein solutions. Specific binding of IgG is detected electronically (some NSB is observed for 100 nM SA, but the signal is much smaller than that of IgG).

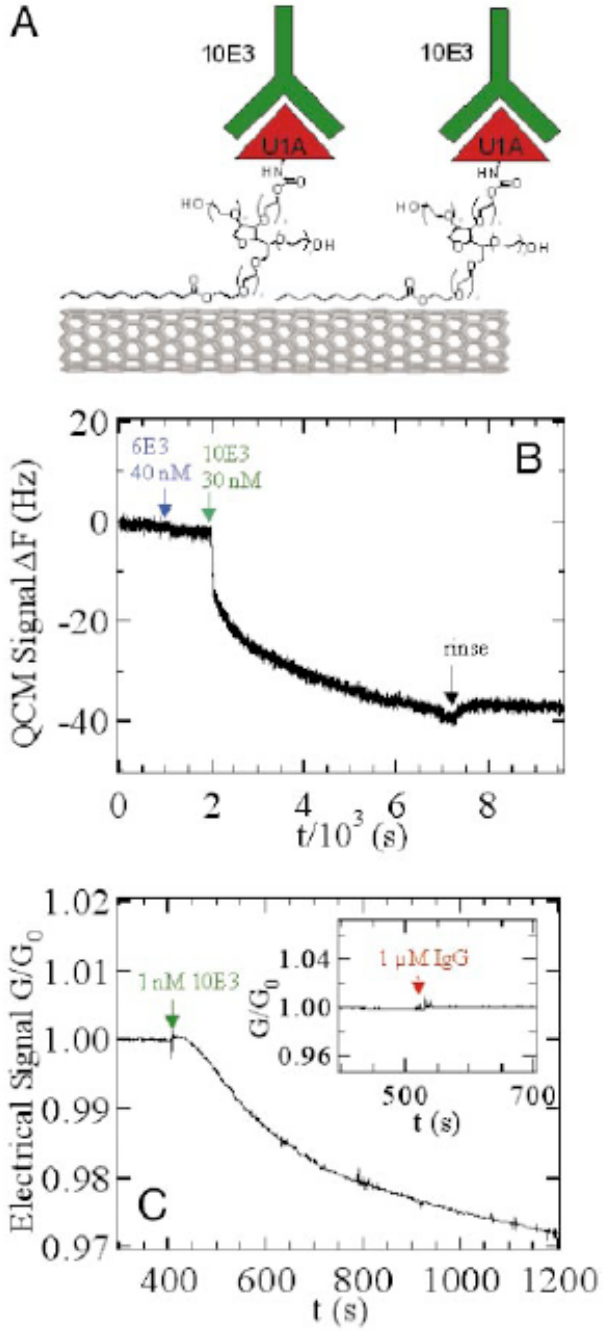

Other CNT biosensor results:

- Vertically alligned CNT arrays.
- Antibodies raised against CNT and C_{60}.
- Electropolymerization of conducting polymers.

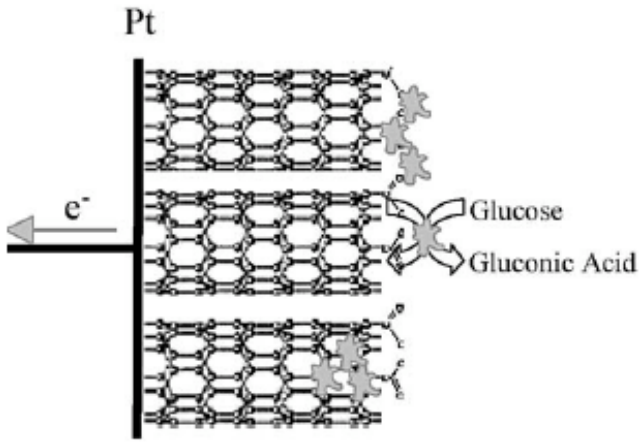

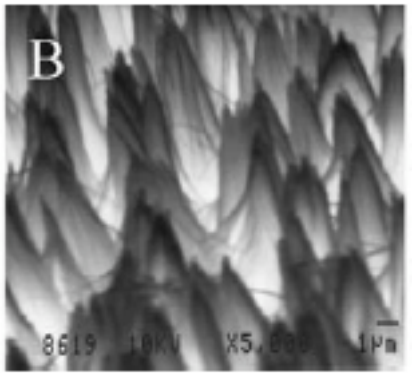

Single-Wall Carbon Nanotubes for Nanoelectronics & Biosensors

- SWNT devices
- SWNT circuits
- Interactions with proteins and DNA
- Self-assembly using DNA
- Biosensors from protein/CNT

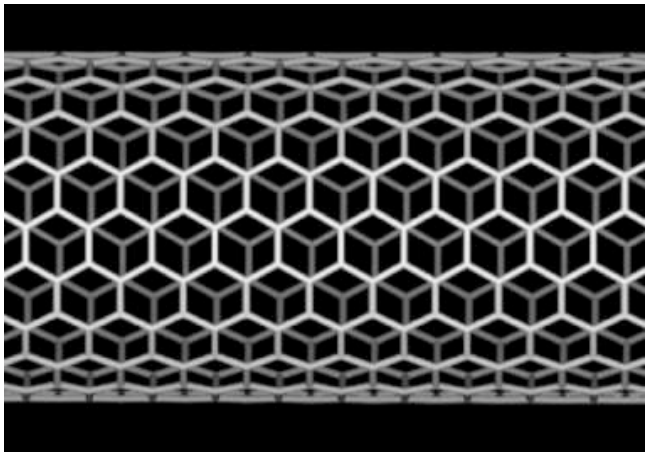

(10,10) SWNT

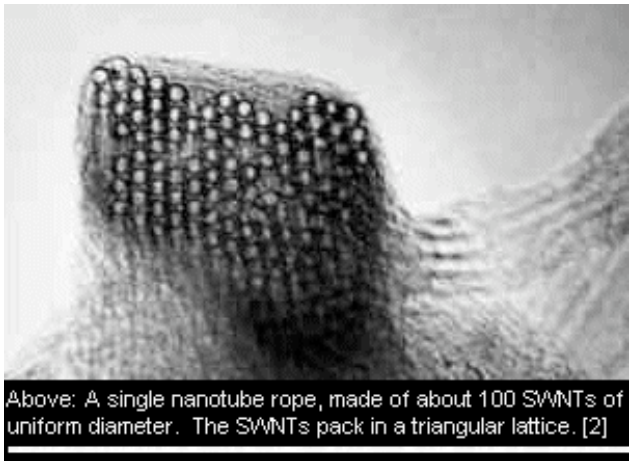

Above: A single nanotube rope, made of about 100 SWNTs of uniform diameter. The SWNTs pack in a triangular lattice. [2]

Metallic nanowires templated on DNA

DNA-templated assembly and electrode attachment of a conducting silver wire

Erez Braun*, Yoav Eichen†‡, Uri Sivan*‡
& Gdalyahu Ben-Yoseph*‡

* Department of Physics, † Department of Chemistry, ‡ Solid State Institute, Technion-Israel Institute of Technology, Haifa 32000, Israel

NATURE | VOL 391 | 19 FEBRUARY 1998 775-778

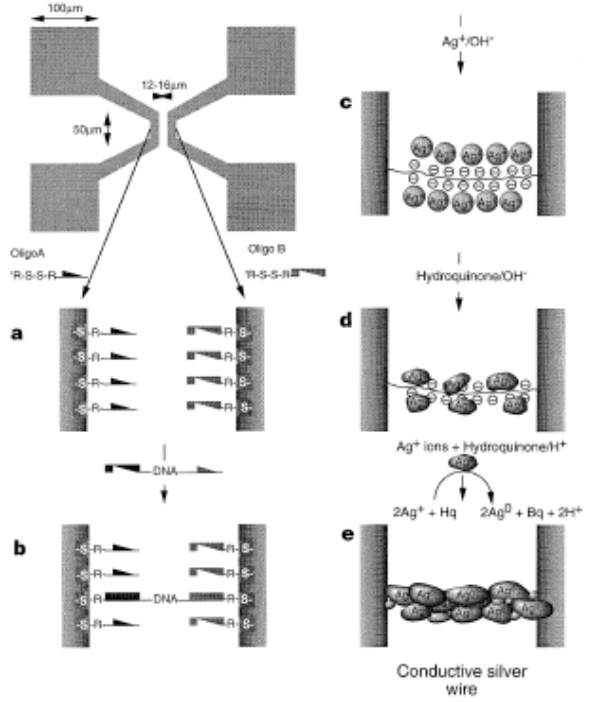

Figure 1 Construction of a silver wire connecting two gold electrodes. The top left image shows the electrode pattern (0.5 × 0.5 mm) used in the experiments. The two 50 μm long, parallel electrodes are connected to four (100 × 100 μm) bonding pads. **a**, Oligonucleotides with two different sequences attached to the electrodes. **b**, λ-DNA bridge connecting the two electrodes. **c**, Silver-ion-loaded DNA bridge. **d**, Metallic silver aggregates bound to the DNA skeleton. **e**, Fully

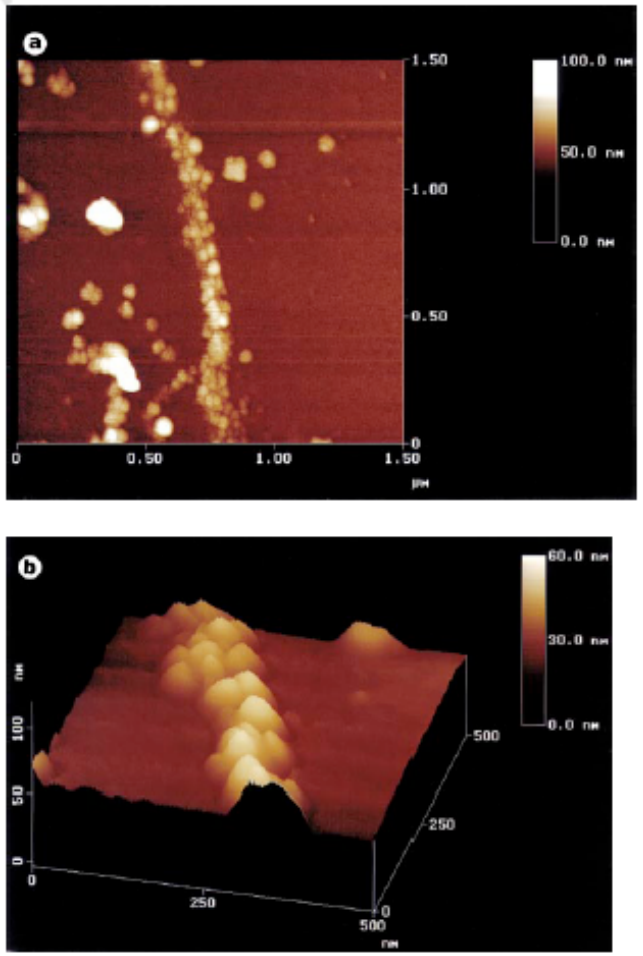

Figure 3 Atomic force microscopy images (Dimension 3000, Digital Instruments) of a silver wire connecting two gold electrodes 12 μm apart. **a**, 1.5 μm; **b**, 0.5 μm field sizes. Note the granular morphology of the conductive wire.

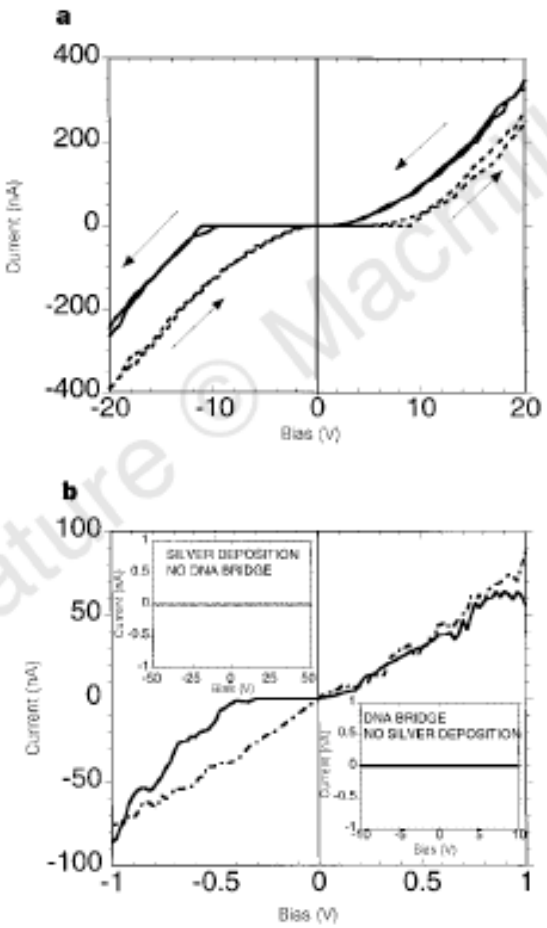

Figure 4 Experimentally observed *I*–*V* curves. **a**, Two terminal *I*–*V* curves of the silver wire shown in Fig. 3. Arrows indicate voltage scan direction. The two curves in each direction present repeated measurements thus demonstrating the stability of a given wire. Note the different asymmetry pertaining to the two scan directions. **b**, *I*–*V* curves of a different silver wire in which the silver growth was more extensive than in **a**. Extensive growth resulted in a narrower current plateau (solid curve), on the order of 0.5 V, and a lower differential resistance (7 MΩ versus 30 MΩ in **a**). By applying 50 V to the wire, the plateau has been permanently eliminated to give an ohmic behaviour (dashed-dotted line), over the whole measurement range. *I*–*V* curves of a DNA bridge with no silver deposition, and silver deposition without a DNA bridge, are depicted in the bottom and top insets, respectively. In both cases, the sample is insulating.

. Here we describe a two-step procedure that may allow the application of DNA to the construction of functional circuits. In our scheme, hybridization of the DNA molecule with surface-bound oligonucleotides is first used to stretch it between two gold electrodes; the DNA molecule is then used as a template for the vectorial growth of a 12 μm long, 100 nm wide conductive silver wire. The experiment confirms that the recognition capabilities of DNA can be exploited for the targeted attachment of functional wires.

NATURE | VOL 391 | 19 FEBRUARY 1998 775-778

Sequence-Specific Molecular Lithography on Single DNA Molecules

Kinneret Keren,[1] Michael Krueger,[1] Rachel Gilad,[1] Gdalyahu Ben-Yoseph,[1,2] Uri Sivan,[1,2] Erez Braun[1,2]*

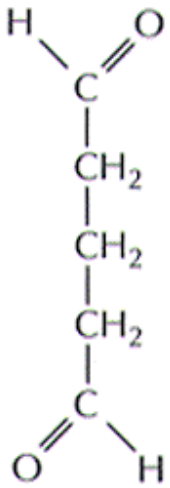

glutaraldehyde

Recent advances in the realization of individual molecular-scale electronic devices emphasize the need for novel tools and concepts capable of assembling such devices into large-scale functional circuits. We demonstrated sequence-specific molecular lithography on substrate DNA molecules by harnessing homologous recombination by RecA protein. In a sequence-specific manner, we patterned the coating of DNA with metal, localized labeled molecular objects and grew metal islands on specific sites along the DNA substrate, and generated molecularly accurate stable DNA junctions for patterning the DNA substrate connectivity. In our molecular lithography, the information encoded in the DNA molecules replaces the masks used in conventional microelectronics, and the RecA protein serves as the resist. The molecular lithography works with high resolution over a broad range of length scales from nanometers to many micrometers.

5 JULY 2002 VOL 297 SCIENCE 72-75

5 JULY 2002 VOL 297 SCIENCE 72-75

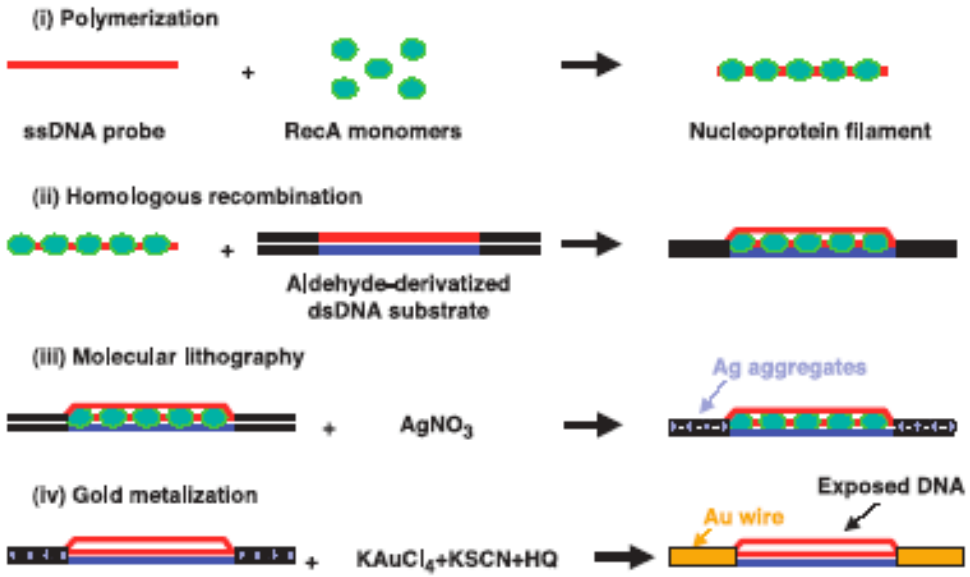

Fig. 1. Schematics of the homologous recombination reaction and molecular lithography. In part (i), RecA monomers polymerize on a ssDNA probe molecule to form a nucleoprotein filament. In part (ii), the nucleoprotein filament binds to an aldehyde-derivatized dsDNA substrate molecule at a homologous sequence. In part (iii), incubation in $AgNO_3$ solution results in the formation of Ag aggregates along the substrate molecule at regions unprotected by RecA. In part (iv), the Ag aggregates serve as catalysts for specific gold deposition, converting the unprotected regions to conductive gold wires. HQ, hydroquinone.

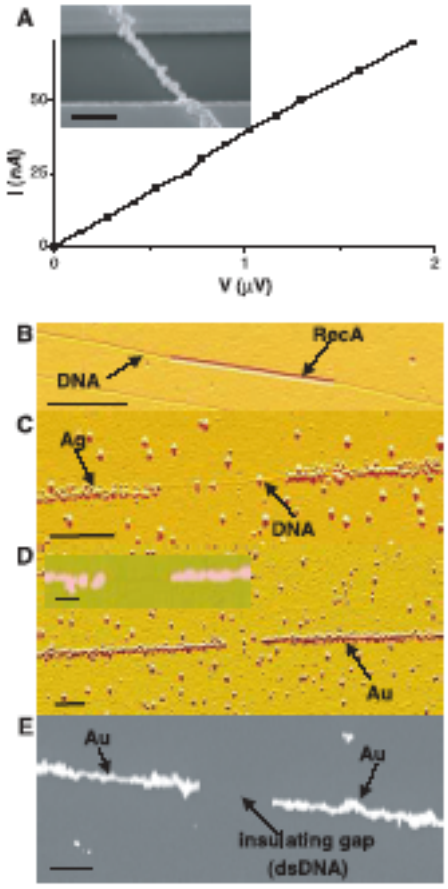

Fig. 2. Sequence-specific molecular lithography on a single DNA molecule. (A) Two-terminal current-voltage (I-V) curve of a DNA-templated gold wire. The wire's resistivity is 1.5×10^{-7} ohm·m, and that of polycrystalline gold is 2.2×10^{-8} ohm·m. Inset, SEM image of a typical DNA-templated wire stretched between two electrodes deposited by e-beam lithography. Scale bar, 1 μm. (B) AFM image of a 2027-base RecA nucleoprotein filament bound to an aldehyde-derivatized λ-DNA substrate molecule. (C) AFM image of the sample after Ag deposition. DNA is exposed at the gap between the Ag-loaded sections. (D) AFM image of the sample after gold metallization. Inset, close-up image of the gap. The height of the metallized sections is ~50 nm. (E) SEM image of the wire after gold metallization. Scale bars in (B) through (E), 0.5 μm; scale bar in inset to (D), 0.25 μm. The distribution in the gap's

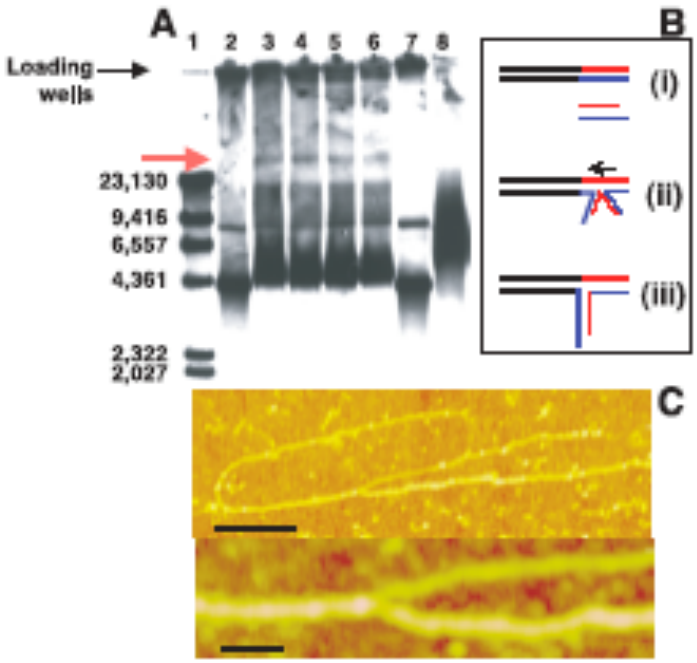

Fig. 4. Stable three-armed junction. (A) RecA-promoted homologous junction formation (*12*) between biotin-labeled 4.3-kbp-long and unlabeled 15-kbp-long dsDNA molecules. The reaction products for different reaction times (lane 3, 30 min; lane 4, 60 min; lane 5, 120 min; lane 6, 210 min) were electrophoresed, blotted onto a nylon membrane, and detected with a chemiluminescent-biotin detection kit. Lane 1, biotin-labeled Hind III–digested λ-DNA marker. Lanes 2 and 7 are control reactions without RecA (lane 2, 5 min; lane 7, 210 min). Lane 8 is a control reaction without ATP (210 min). The band marked by a red arrow contains stable three-armed junctions. Additional bands correspond to labeled 4.3-kbp molecules and their 8.6-kbp spontaneously formed dimers. At long reaction times (lanes 5 and 6), the junction band intensity decreases because of junction-junction interaction leading to the formation of more complex structures that remain in the loading wells. (B) Different steps in junction formation. Step (i) shows building blocks (15-and 4.3-kbp dsDNA). The latter molecule is completely homologous to one end of the former molecule and has a 50-base-long sticky end (*12*). Step (ii) shows pairing at homologous sequences and branch migration. Step (iii) shows the final product, a stable three-armed junction. (C) AFM images of a three-armed junction, which can serve as a scaffold for a three-terminal device. Scale bars, 0.25 μm (top) and 50 nm (bottom). The lengths of the arms are as expected, considering the variations due to interaction with the surface in the combing process.

DNA-Templated Carbon Nanotube Field-Effect Transistor

Kinneret Keren,[1] Rotem S. Berman,[1] Evgeny Buchstab,[2]
Uri Sivan,[1,2] Erez Braun[1,2]*

The combination of their electronic properties and dimensions makes carbon nanotubes ideal building blocks for molecular electronics. However, the advancement of carbon nanotube–based electronics requires assembly strategies that allow their precise localization and interconnection. Using a scheme based on recognition between molecular building blocks, we report the realization of a self-assembled carbon nanotube field-effect transistor operating at room temperature. A DNA scaffold molecule provides the address for precise localization of a semiconducting single-wall carbon nanotube as well as the template for the extended metallic wires contacting it.

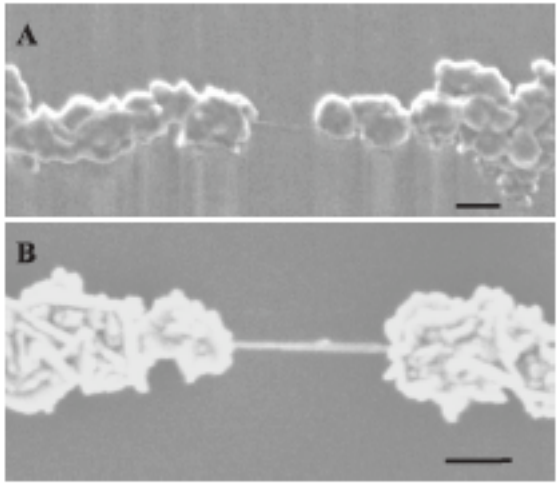

Fig. 3. A DNA-templated carbon nanotube FET and metallic wires contacting it. SEM images of SWNTs contacted by self-assembled DNA-templated gold wires. (A) An individual SWNT. (B) A rope of SWNTs. Bars, 100 nm.

21 NOVEMBER 2003 VOL 302 SCIENCE 1380-1382

Fig. 1. Assembly of a DNA-templated FET and wires contacting it. Steps are as follows: (i) RecA monomers polymerize on a ssDNA molecule to form a nucleoprotein filament. (ii) Homologous recombination reaction leads to binding of the nucleoprotein filament at the desired address on an aldehyde-derivatized scaffold dsDNA molecule. (iii) The DNA-bound RecA is used to localize a streptavidin-functionalized SWNT, utilizing a primary antibody to RecA and a biotin-conjugated secondary antibody. (iv) Incubation in an $AgNO_3$ solution leads to the formation of silver clusters on the segments that are unprotected by RecA. (v) Electroless gold deposition, using the silver clusters as nucleation centers, results in the formation of two DNA-templated gold wires contacting the SWNT bound at the gap.

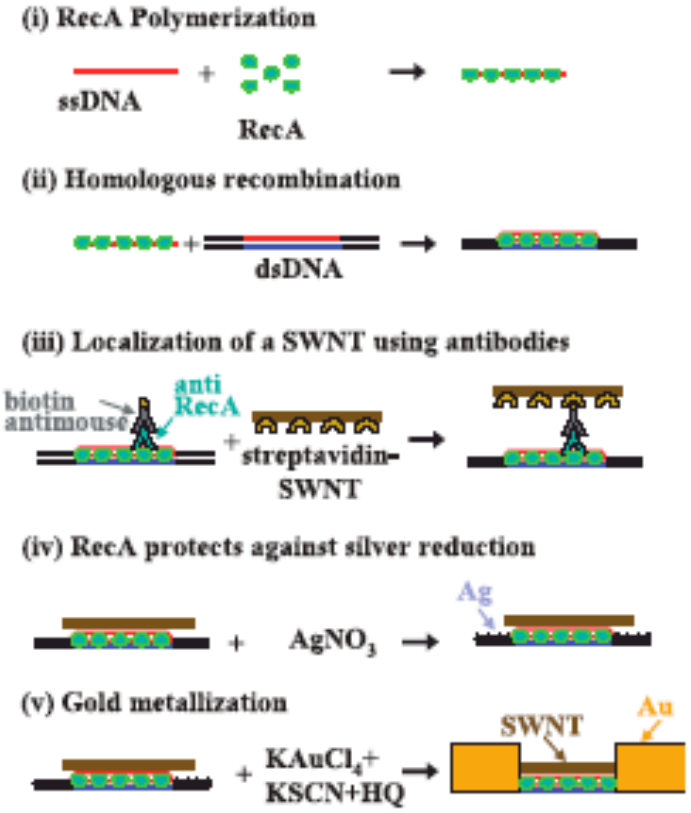

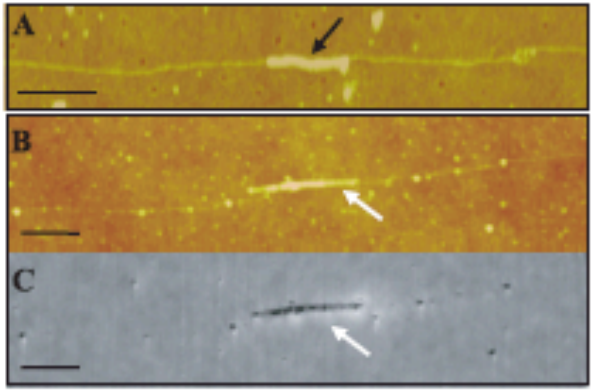

Fig. 2. Localization of a SWNT at a specific address on the scaffold dsDNA molecule using RecA. (**A**) An AFM image of a 500-base-long (~250 nm) RecA nucleoprotein filament (black arrow) localized at a homologous sequence on a λ = DNA scaffold molecule. Bar, 200 nm. (**B**) An AFM image of a streptavidin-coated SWNT (white arrow) bound to a 500-base-long nucleoprotein filament localized on a λ-DNA scaffold molecule. Bar, 300 nm. (**C**) A scanning conductance image of the same region as in (**B**). The conductive SWNT (white arrow) yields a considerable signal whereas the insulating DNA is hardly resolved. Bar, 300 nm. Phase shift limits, 0° to 20° (*20*).

21 NOVEMBER 2003 VOL 302 SCIENCE 1380-1382

21 NOVEMBER 2003 VOL 302 SCIENCE 1380-1382

- Self-assembled FET.
- Assembly errors...
- Contact resistance...
- Hysteresis...

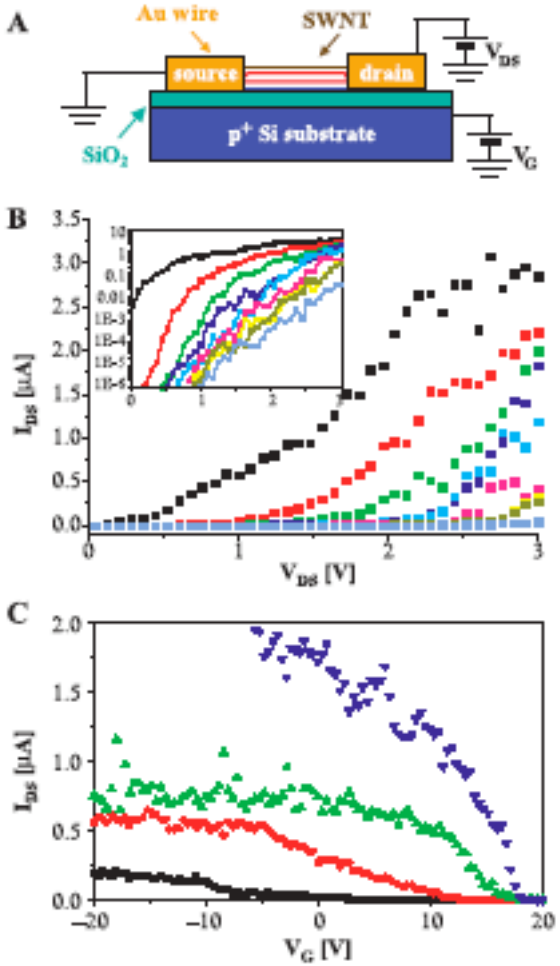

Fig. 4. Electrical characteristics of the DNA-templated carbon nanotube FET. (**A**) Schematic representation of the electrical measurement circuit. (**B**) Drain-source current (I_{DS}) versus drain-source bias (V_{DS}) for different values of gate bias (V_G). V_G = –20 V (black), –15 V (red), –10 V (green), –5 V (blue), 0 V (cyan), 5 V (magenta), 10 V (yellow), 15 V (olive), 20 V (slate blue). The inset depicts the same data on a logarithmic scale. (**C**) Drain-source current versus gate voltage for different values of drain-source bias [same device as (B)]. V_{DS} = 0.5 V (black), 1 V (red), 1.5 V (green), 2 V (blue).

Bacteriophage-λ DNA has been used as a template for the deposition of various metals including:

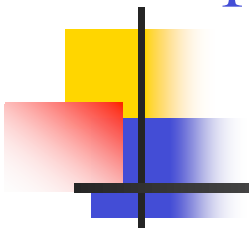

- Silver: E. Braun, Y. Eichen, U. Sivan, G. Ben-Yoseph, *Nature* **391**, 775 (1998).
- Gold: K. Keren, *et al*., *Science*, **297**, 72 (2002).
- Gold: F. Patolsky, Y. Weizmann, O. Lioubashevski, I. Willner, *Angew. Chem.-Int. Edit.* **41**, 2323 (2002).
- Copper: C.F. Monson, A.T. Woolley, *Nano Lett.* **3**, 359 (2003).
- Platinum: W.E. Ford, O. Harnack, A. Yasuda, J.M. Wessels, *Adv. Mater.* **13**, 1793 (2001).
- Palladium: J. Richter, *et al*., *Adv. Mater.* **12**, 507 (2000).

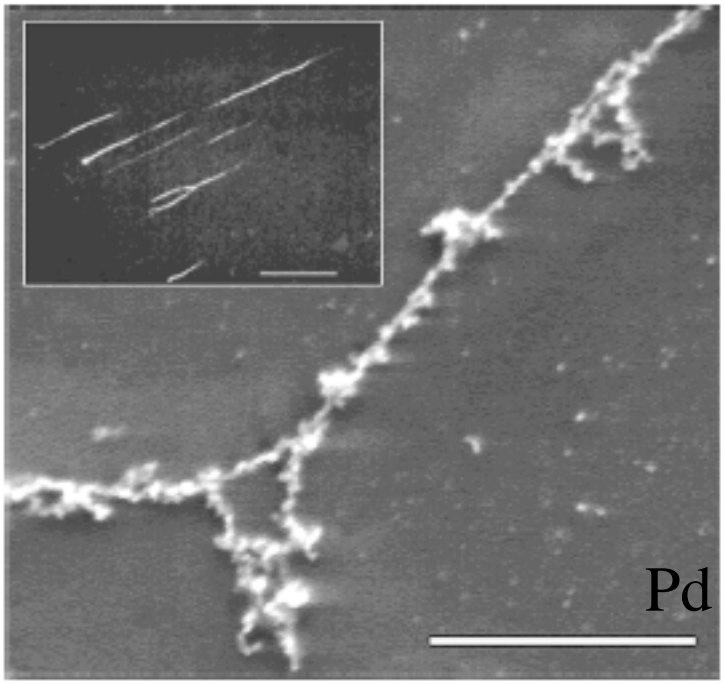

Fig. 3. SEM picture of a metallized DNA strand 40 nm thick on a glass surface. The DNA was aligned by evaporating a drop of DNA solution and metallized afterwards. For better visualization the sample was covered with 1 nm carbon (scale bar 1 μm). Inset: Parallel aligned fluorescence-labeled DNA strands before metallization (scale bar 10 μm).

Adv. Mater. **2000**, *12*, No. 7

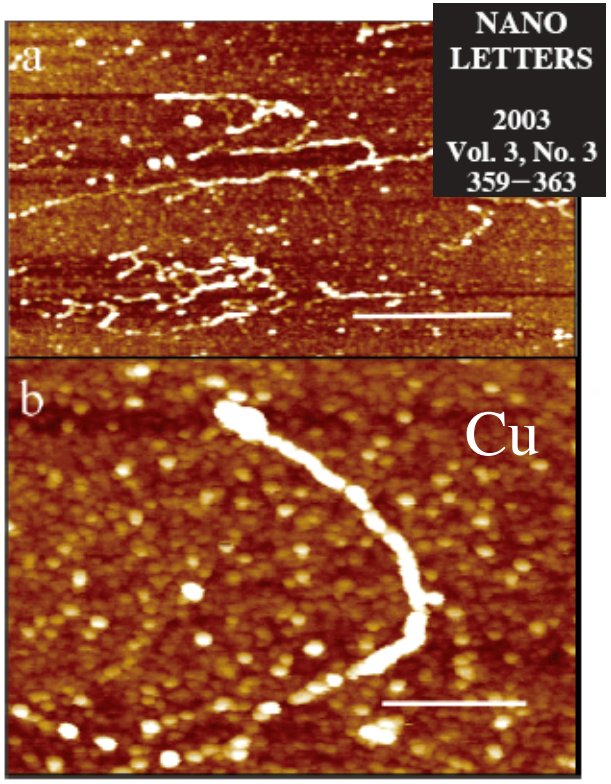

Figure 3. AFM height images of λ DNA deposited on silicon and treated twice with copper(II) nitrate and ascorbic acid. (a) Image

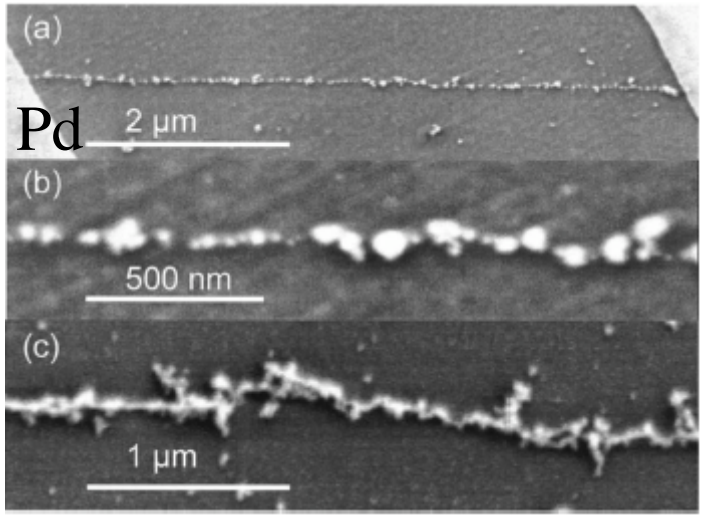

APL, 78, 536-538 (2001)

DNA-Templated Self-Assembly of Protein Arrays and Highly Conductive Nanowires

Hao Yan,[1*] Sung Ha Park,[1,2] Gleb Finkelstein,[2] John H. Reif,[1] Thomas H. LaBean[1*]

26 SEPTEMBER 2003 VOL 301 SCIENCE 1882-1885

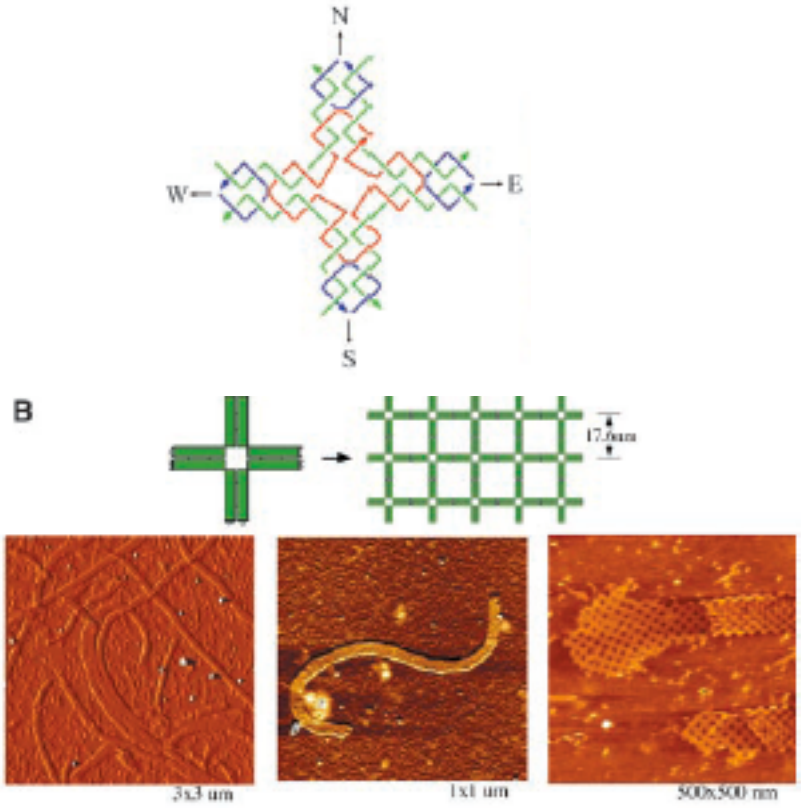

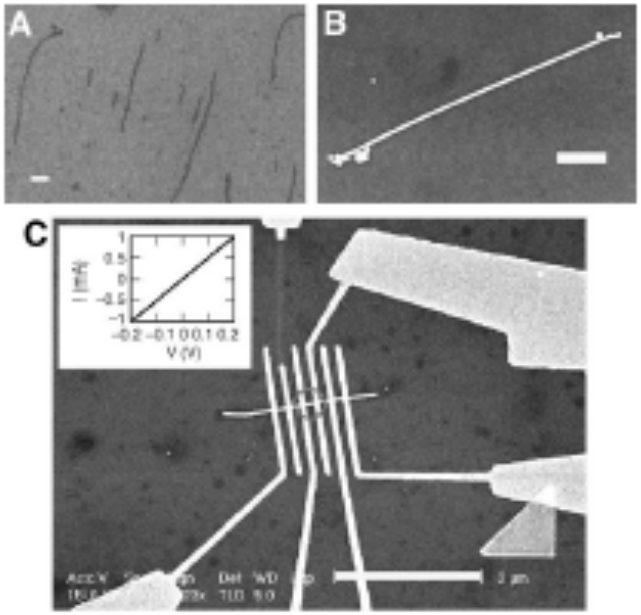

Fig. 3. Metallization and conductivity measurements of metallized 4 × 4 ribbons. (A) SEM image of nonmetallized 4 × 4 DNA nanoribbons (scale bar: 500 nm). (B) SEM image of silver-seeded silver nanoribbon (scale bar: 500 nm). The change in the signal contrast between (A) and (B) is apparent. (C) SEM image of the actual device (scale bar: 2 μm). (Inset) Current-voltage curve of the silver-seeded silver 4 × 4 nanoribbon.

DNA nanotubes self-assembled from triple-crossover tiles as templates for conductive nanowires

Dage Liu*, Sung Ha Park*†, John H. Reif*, and Thomas H. LaBean*‡

PNAS | January 20, 2004 | vol. 101 | no. 3 | 717–722

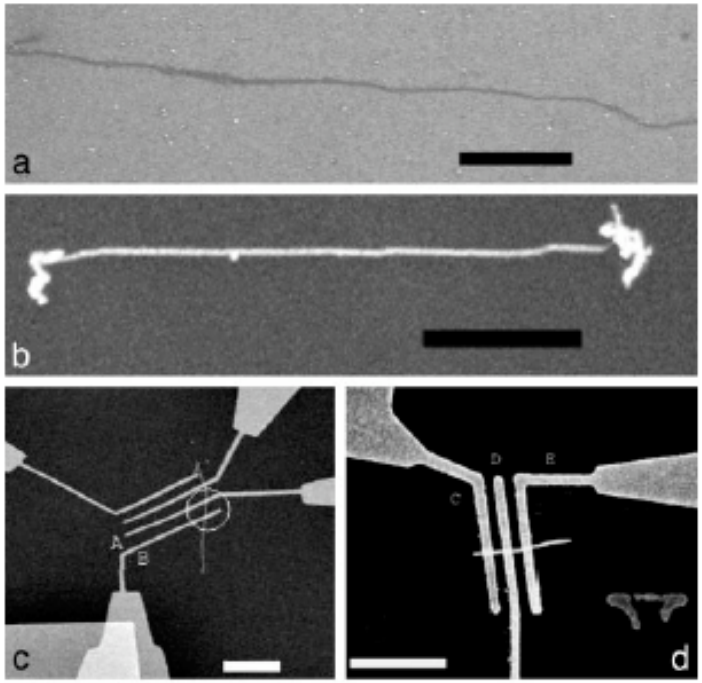

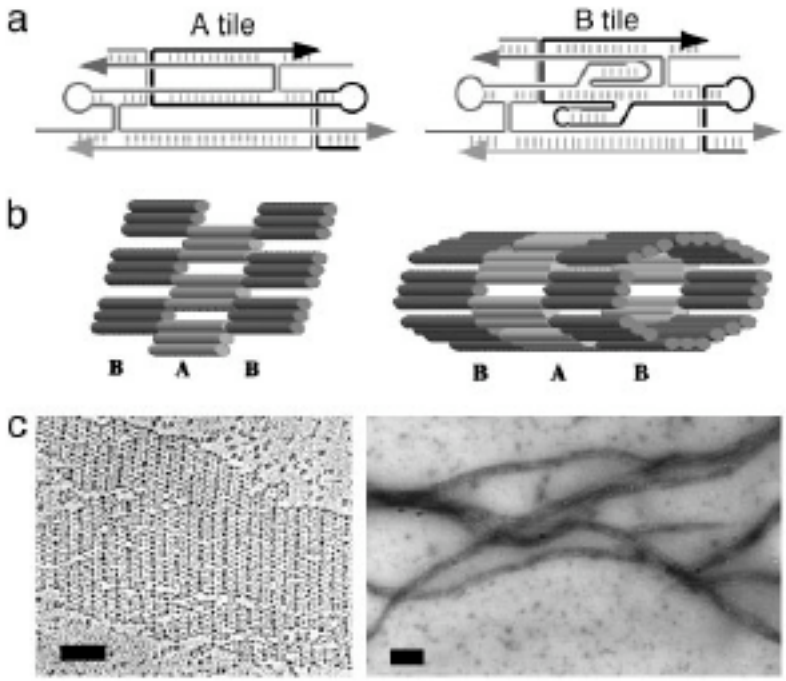

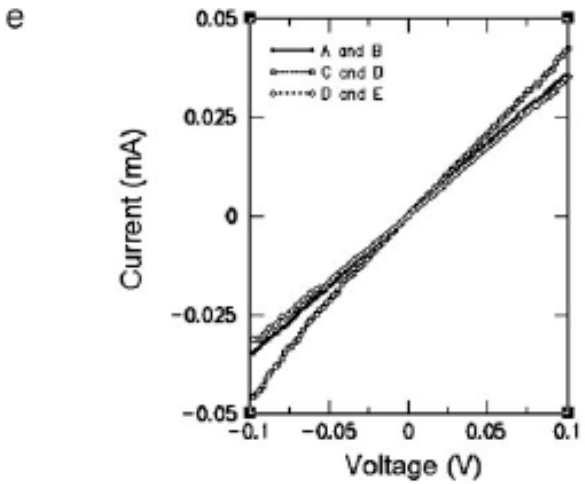

DNA-Templated Fabrication of 1D Parallel and 2D Crossed Metallic Nanowire Arrays

NANO LETTERS
2003
Vol. 3, No. 11
1545−1548

Zhaoxiang Deng and Chengde Mao*

Department of Chemistry, Purdue University, West Lafayette, Indiana 47907

This paper reports a simple method for the fabrication of ordered nanostructures composed of metallic nanowires. Molecular combing was used to stretch and align linear λ-DNA molecules into parallel or crossed patterns. Subsequent metallization of DNA through electroless palladium deposition yielded 1D parallel or 2D crossed metallic nanowire arrays. This method has potential use in building interconnects between nanosized building blocks toward nanodevice construction.

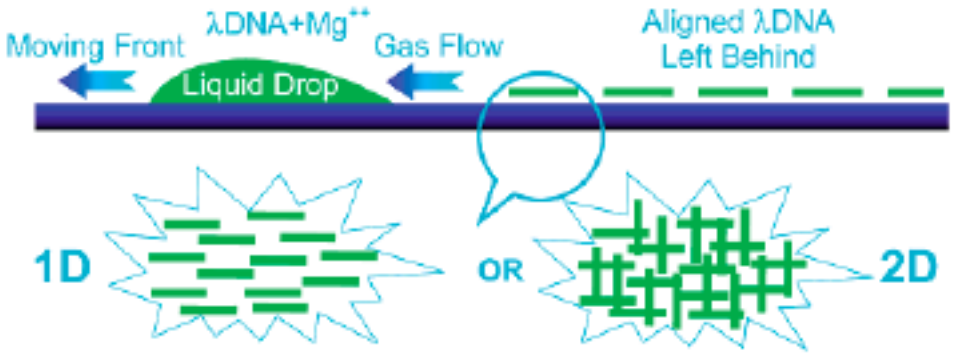

Figure 1. Schematic representation of the fluid-flow-assisted molecular combing of DNA molecules on a surface.

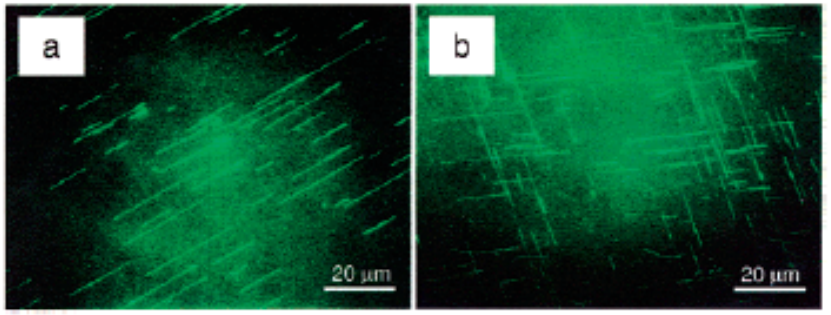

Figure 2. Fluorescence microscopy pictures showing (a) 1D- and (b) 2D-aligned DNA wires formed by fluid-flow-induced molecular combing.

NANO
LETTERS

2003
Vol. 3, No. 11
1545−1548

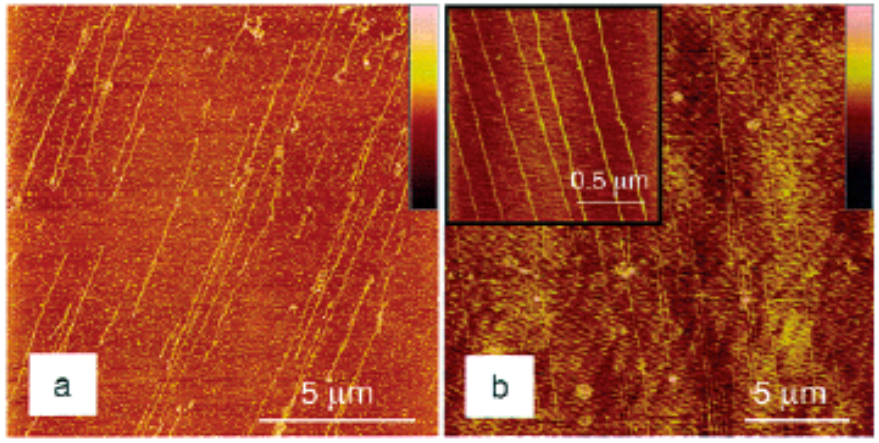

Figure 3. AFM images of (a) 1D-aligned Pd nanowires and (b) the corresponding precursory DNA molecules. The inset in b gives a detailed view of the parallel DNA duplexes. Height scale: (a) 15 nm and (b) 1.0 nm.

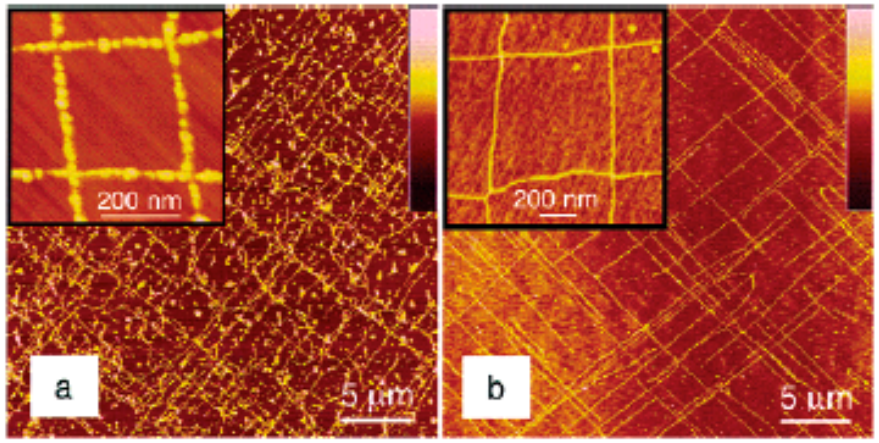

Figure 4. AFM images of (a) 2D-aligned Pd nanowires and (b) the corresponding precursory DNA molecules. The insets in a and b give enlarged views of 2D squares of metal nanowires and DNA molecules, respectively. Height scale: (a) 30 nm and (b) 3.0 nm.

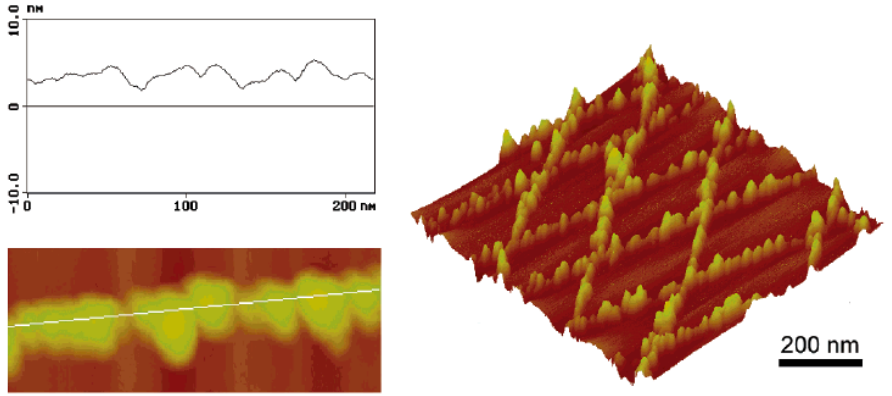

Figure 5. Left: high-magnification AFM image of a Pd nanowire; a section analysis of it shows an average particle height of about 5 nm. Right: high-magnification image of a meshlike 2D array of Pd nanorwires formed by the metallization of a 2D-aligned DNA sample.